Master Thesis

Double resonance Raman spectra of G′ and G* bands of graphene

（グラフェンにおける G′ バンドと G* バンドの二重共鳴ラマン分光）

Syahril Siregar

Department of Physics, Graduate School of Science
Tohoku University

September 2015

Acknowledgments

I would like to use this opportunity to thank many people who contributed to this master thesis over the two years of my master course studies at Tohoku University. First of all, I would like to express my sincere thanks to my supervisor, Prof. Riichiro Saito for accepting me into his group and for his guidance. I would like to thank Dr. A.R.T. Nugraha for teaching me a lot of basic physics behind my research and also his hospitality support during my stay in Japan. Thank you to Hasdeo-san for his support in my weekly report. I would like to thank all the members of the Saito group; Shoufie-san, Pourya-san, Thomas-san, Nguyen-san, Inoue-san, Mizuno-san, Shirakura-san, and Tatsumi-san. Special thanks to Pourya-san, who help me to calculate phonon energy dispersion by using quantum espresso package.

I am indebted to Indonesia endowment fund for education, ministry of finance Republic of Indonesia (LPDP) for financing my study in Japan.

I address my best regards also to some professor in my previous university, University of Indonesia; Muhammad Aziz Majidi, Ph.D., Prof. Rosari Saleh, Dr. Dede Djuhana, and Dr. Muhammad Hikam who gave me outstanding encouragement to study abroad. Lastly, I thank my family for their continuous support.

Contents

Chapter 1

Introduction

1.1 Purpose of the study

Graphene is a two-dimensional (2D) material of carbon in a honeycomb lattice. The electronic structure of graphene is already calculated in 1947 by P. R. Wallace [1]. He found that the electronic structure of graphene shows no energy gap between the valence and conduction bands, while, the valence and conduction bands do not overlap each other. Its electronic structure also shows the linear electronic dispersion, unlike the most materials whose energy dispersions are quadratic of k.

In order to study the graphene, we need tools for characterization of the sample. Raman spectroscopy is a very useful tool for evaluating sample, because from Raman spectra we can obtain a lot of important informations, such as, the number of graphene layers [2], the presence of the deffect or disorder [3], the atomic doping impurity [4], and the existence of strain [5].

In this master thesis, we explain the effect of the laser excitation energy (E_L) from infrared to deep ultraviolet (UV) to the the Raman spectra, especilally for G$'$ band. The second purpose of this thesis is to assigned G* band and calculate Raman intensity of G* band. Therefore we can prove our models to calculate Raman intensity is acceptable, and we can use the

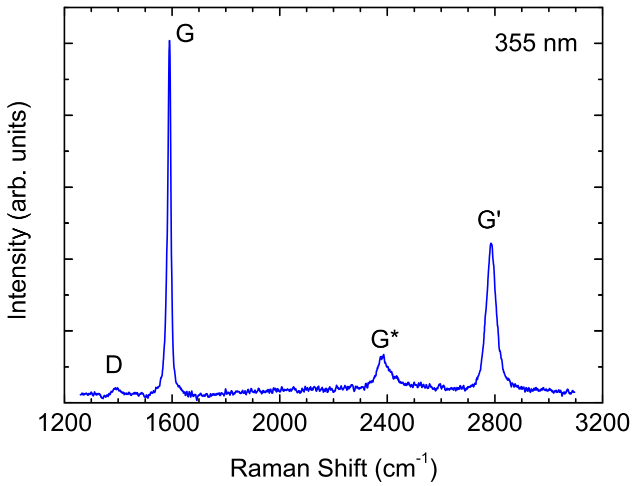

Figure 1.1 Raman spectra of monolayer graphene on a sapphire substrate excited by 355 nm laser [7]. There are four peaks appear; D band, G band, G′ band, and G* band.

models to calculate Raman intensity for different condition in the future.

Raman spectroscopy is inelastic scattering of light by matter [6]. Inelastic scattering means that the energies incoming photon and the outgoing photon are not the same. The shift of the energy is called Raman shift. The Raman shift is the finger print of the Raman spectroscopy, because it has some information about atomic vibration, electronic energy, etc. Combination of experiment with calculation is important for understanding Raman spectroscopy, because some concepts of basic solid state physics are needed for explaining Raman spectra as a function of many experimental parameters, such as laser excitation energy, temperature, pressure, and Fermi energy of materials [6].

In Fig. 1.1, we show the typical experimental result of Raman spectra of monolayer graphene excited by 355 nm laser. There are four peaks exist

---

Fig. 1.1: picuse/ramanexpe.eps

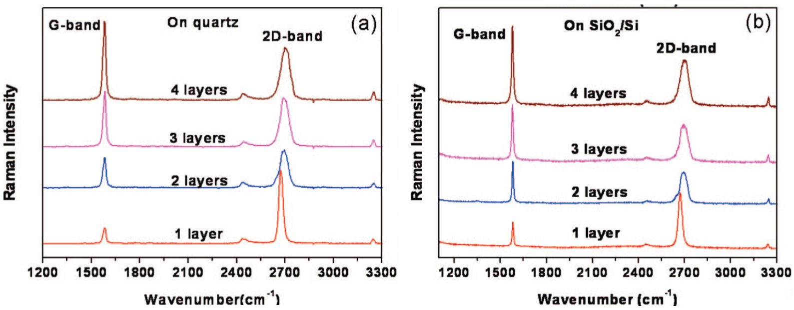

Figure 1.2 The experimental results of Raman spectra of monolayer, bilayer, three layers, and four layers graphene on (a) quartz and (b) SiO$_2$ substrate excited by 532 nm laser [12].

in the Raman spectra of monolayer graphene, such as; D , G, G*, and G$'$ bands, however, only two intrinsic peaks in Raman spectra of monolayer graphene are G band and G$'$ bands [6], which are free from impurity or defects, while the D band is a defect oriented peak and G* band origin is not well understood. The G band peak lies around 1580 cm^{-1} and G$'$ band exists around 2700 cm^{-1}, the D band frequency is 1350 cm^{-1} and G* band is 2400 cm^{-1}.

From the G band, we can get information about the sample, such as ; existence of strain, effect of gate doping, and the impurity. Since the peak position of G band is sensitive to the gate voltage applied to graphene, we can evaluate the Fermi energy by peak position [8]. The G$'$ band also has very important information for sample characterization. We can obtain information about the number of graphene layers, temperature, and the order of stacked graphene [3, 9, 10, 11].

Although the Raman spectroscopy is very important for evaluating sample, and the intensity ratio of G$'$ to G band is frequently used for characterizing the number of layer of graphene [13], the discussion of G$'$ band without information about E_L does not have a meaning, because recently

---

Fig. 1.2: picuse/figmultilayer.eps

experimental result done by Liu *et al.* reported the G$'$ band frequency and intensity is sensitive to the E_L [7].

Based on experimental result in Fig. 1.1 there are four bands exist. The origin of D, G, and G$'$ bands process are already known. However, we still have another peak, its intensity is very small. This peak position is around 2400 cm^{-1} which called G* band. The origin of G* band is still debatable, because previous work assigned the G* band and calculated Raman intensity but, previous work did not reproduce the experimental result [8, 14, 15]. The G* band exists in single and multilayer graphene as shown in Fig. 1.2. The existence of G* band in monolayer graphene and related materials on various substrate have been pointed out from previous work [8, 12, 14].

In order to understand Raman spectroscopy, theoretical approach is needed. The theory to calculate Raman spectra is done by our group [16, 17, 18, 19, 20].

G band is the first-order Raman process, and the G$'$ band is double resonance Raman process [3, 6, 13, 19]. However, the study of Raman spectra of graphene as a function of laser energy has not complete yet, such as the effect of using deep ultraviolet laser energy to the behavior of peak.

1.2 Organization

This thesis is organized into seven chapters. In the chapter 1, we explain the purpose of the study. In chapter 2, we introduce the background and motivation for understanding this thesis. In chapter 3, the structure of graphene, the vibrational properties ,the electronic band structures of graphene based on simple and extended tight binding approximation are reviewed. In chapter 4, we describe the calculation methods used in this thesis. The formula to calculate Raman intensity is introduced. The electron-photon interaction matrix is briefly reviewed, which was previously developed by J. Jiang *et al.* [21] and A. Grüneis *et al.* [22] in our group. We will explain the calculation result about the $\mathrm{G}^\star$ band in chapter 5. The calculation result about the G' band will be disscused in chapter 6. The effect of deep ultraviolet laser energy is also discussed in chapter 6. Finally in chapter 7, summary of this thesis will be given.

Chapter 2

Background

In this chapter, we review some important backgrounds that motivated the present work. We will start from the recently experimental result of monolayer graphene then we explain the general concept of Raman spectroscopy in monolayer graphene.

2.1 Experimental Raman spectra of monolayer graphene

Recently Hsiang-Lin Liu *et al.* measured the Raman spectra of monolayer graphene for several laser excitation energy [7]. He used a liquid-nitrogen-cooled charge- coupled detector (CCD) camera with $f = 500$ mm spectrometer by installing an 1800 lines/mm grating (princeton instruments, Inc.). The excitation laser 266 nm and 355 nm was focused onto the sample by an objective lens (0.5 N.A., 40×, Thorlabs, Inc.). Additionally for visible light, 532 nm and 785 nm, the laser was focused by objective lens (0.95 N.A.). The power of the all lasers is 1.0 mW to avoid the heating effect which can damage the sample [7]. The Raman spectra measurements were measured at room temperature. Fig. 2.1(a) shows the Raman spectra of monolayer graphene on a sapphire substrate excited by deep-ultraviolet 266 nm (4.66 eV), ultraviolet 355 nm (3.49 eV), visible 532 nm (2.33 eV), and near-infrared

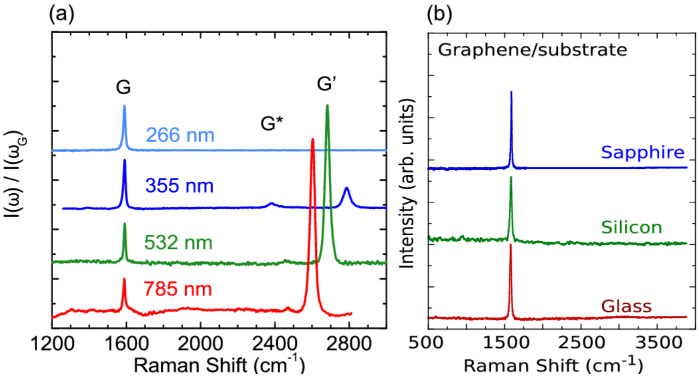

Figure 2.1 The experimental result of Raman scattering spectra of monolayer graphene (a) on sapphire substrate excited by 266 nm, 355 nm, 532 nm, and 785 nm laser excitation energy and (b) on three different substrate excited by 266 nm laser excitation energy [7].

(1.58 eV) laser energies, the spectra were normalized to the G band intensity for each laser energy. Fig. 2.1(a) shows there are three peaks. G, G*, and G$'$ bands. The G band exists at 1582 cm^{-1} in all laser energy. The G* band intensity are very weak and exist around 2400 cm^{-1}, these peaks shifts as a function of laser energy. The G* band peak position shifts to the lower Raman shift with increasing laser energy.

The G$'$ band exists around 2700 cm^{-1}. The peak position of G$'$ band shifts as a function of laser energy whose slope is opposite to the G* band, the slope of G$'$ band is 85-107 cm^{-1}/eV [23, 24, 25] while the slope of G* band is -10 to -20 cm^{-1}/eV [23, 26]. The peak intensity of G$'$ band decreases with increasing E_L and disappears in laser energy at 266 nm. This phenomenon is very interesting, because the relative intensity of G$'$ band to G band is used to evaluating the number of graphene layer [13, 27]. Therefore the information about used laser energy in Raman spectra of graphene becomes very important.

Because the frequency of G$'$ band is about twice of D band frequency, the

---

Fig. 2.1: picuse/ramanexp.eps

G′ band is also called the 2D band in the carbon literature [28, 29], but G′ band is most popular name because, G′ band is not a defect process, while the D band denotes the defect peak [6].

In Fig. 2.1(b), we show the Raman spectra of monolayer graphene excited by 266 nm laser in various substrates, such as sapphire, silicon, and glass. G band exists in all substrate and G′ band peaks are absent. Therefore the absence of G′ band is not caused by the effect of substrate.

However, there are only two intrinsic peaks in Raman spectra of monolayer graphene are already known, G band and G′ band [6], which are free from impurity or defects, while the D band is a defect oriented peak [26], and the origin of G⋆ band is not well understood [8, 14, 15].

Because G⋆ band always exist in Raman spectra of graphene and graphene related materials in various of substrate, therefore we know that the G⋆ band is also the intrinsic peak in Raman spectra of monolayer graphene. Previous works about G⋆ band done by T. Shimada *et al.* [14] and Saito *et al.* [8] assigned the G⋆ band based on the phonon energy dispersion, and also one of previous work calculated Raman intensity, therefore can not reproduce the experimental result [8]. However understanding the G⋆ band process is important, because we can prove that the used model to calculate Raman intensity is correct and we can use the model to calculate the raman intensity for various purposes.

Experimental result shows the peak position of G⋆ and G′ bands are sensitive to the laser energy. This behavior usually happen in double resonance Raman process [6].

2.2 Raman spectroscopy in graphene

The inelastic scattering process originates from several physical processes, for example; the vibrations of lattice (phonons) and electron excitations (excitons). In the case of graphene and graphene related materials, phonon

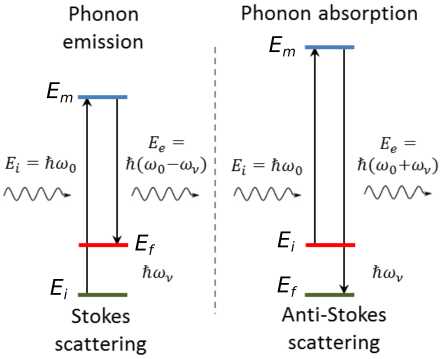

Figure 2.2 Stokes and anti-stokes processes in Raman spectroscopy, stokes process creates a phonon while anti-stokes process destroys a phonon. Anti-stokes signal is usually weaker than the stokes process.

gives the dominant contribution for the observed Raman spectra. In the inelastic scattering, the incident photon can increase or decrease by creating (stokes process) or destroying (anti-stokes) a phonon as shown in Fig.2.2. However, the anti-stokes signal is usually weaker than the stokes process, therefore we just focus on the stokes spectra [6]. The energy axis in the Raman spectra is usually expressed in unit of cm^{-1}. This energy unit is also called the spectroscopic wavenumber and can be calculated using $\nu = \frac{1}{\lambda}$. The energy conversion is 1 eV = 8065.5 cm^{-1}.

In the Raman spectroscopy, the order of Raman process is given by the number of inelastic scattering events of a photo-excited electron [26]. However, there are two most used processes, such as first-order and second-order Raman processes. The first-order Raman process is defined by one phonon emission during the scattering process. The second-order Raman process associated with two phonon emission. Two phonon process can be either overtone of the same phonon mode or combinations of the phonon modes. In this master thesis, we just consider first and second-order Raman processes.

Fig. 2.2: picuse/stokesanti.eps

2.3 First-order Resonance Raman

The first-order Raman process is the Raman process where the photon energy excitation creates one phonon in the crystal with very small momentum $q \approx 0$. The physical process of first-order resonance Raman is explained as follows; an electron with wave-vector $\mathbf{k}$ in an initial state i is excited by an incident photon with energy E_L from the i state to an excited m state by the absorption of an excitation energy $(E_m - E_i)$. If the m state is a real electronic state, the light absorption is the resonance process. This photoexcited electron will be further scattered by a $q \approx 0$ phonon with frequency ω_q to a virtual state m', and decay back to state i by emitting scattered light as shown in Fig. 2.3(a). the detailed explanation about the first-order Raman process will be given in Section 4.1.

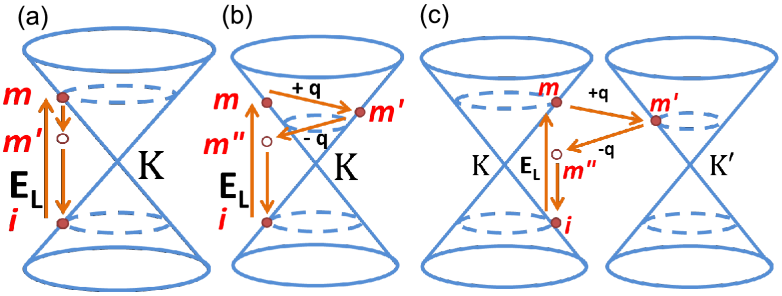

Figure 2.3 The Raman scattering process with laser excitation energy E_L, initial state i, excited state m, and intermediate states m' and m''. (a) One-phonon first-order Raman scattering process. Two-phonon second order resonant Raman processes (b) intravalley (c) intervalley.

2.4 Second-order Raman process

In second-order Raman process, the photo-excited electron is scattered two times. The photo-excited electron is scattered by either emitting a phonon or

---

Fig. 2.3: picuse/firstandsecond.eps

defect process. In this master thesis, we only consider the phonon scattering process.

There are three intermediate electronic states in second order Raman processes (see Fig.2.3(b) and (c)) ; (1) excited state m , (2) the intermediate state m' at $k+q$ at K' point, and (3) the second intermediate state back to the K point, m''. This two-scattering amplitude process is expressed by perturbation theory, in which there are four matrix elements, consist of two for photon absorption and emission, two for phonon emission or absorption (see chapter 3). The denominator consist of three energy difference factor,and these term correspond to energy conservation. We call a process containing two resonance denominators as double resonance Raman [26].

The physical process of second order Raman in graphene is given as follows. Photon with given energy is coming on monolayer graphene, an electron in the valence band excites to the conduction band vertically in momentum space. We always have an electron with wave vector **k** which has resonant condition $E_L = E_c(\mathbf{k}) - E_v(\mathbf{k})$ for any laser energy, because graphene does not has an energy gap. The photo-excited electron with wave vector **k** then scattered by emitting a phonon with wave vector **q** to a state **k - q** as shown in Fig. 2.3 (b) and (c). Then electron scattered to state m'' by emitting the second phonon with wave vector **-q**. Then finally electron comes back to initial state by emitting a photon.

Scattering phonon process can be either intravalley scattering or intervalley scattering. The intravalley scattering process is the scattering process in the same valley, while the intervalley process involves two valley K and K' points in the Brillouin zone. The phonon emission in Fig. 2.3(b) is intravalley and in Fig. 2.3(c) is intervalley scattering, because the phonon wave vector **q** connects two energy bands at the K and K' points in the Brillouin zone. The intensity formula for second-order Raman process will be given in Section 4.1.

2.5 Assignment Raman spectra in graphene

The experimental result of Raman spectra shows there are four peaks, such as D, G,G*, and G$'$ bands as shown in Fig. 1.1. All of these bands were already assigned in previous works. Study about these bands are successful to reproduce the experimental result, however G* band assignment is not established yet. Thus, there was calculation work about G* band, but previous work did not reproduce the experimental result of G* band in monolayer graphene [8, 14, 15].

The D band process is second-order resonance Raman process, it involves one phonon scattering process and one defect, as a consequence the D band is only appear if the defect is exist. The phonon mode correspond to D band is longitudinal optic (LO) or in-plane transverse optic (iTO) modes. In this master thesis, we will not discuss about the D band.

G band process is first-order Raman process. Phonon which contributing to G band is iTO or LO phonon at Γ point, since LO and iTO degenerate in Γ point [6].

Based on previous work, there are four possible assignments for the G* band [8, 14]. previous work mentioned that the G* band is second-order Raman process. The four possible processes are (1) overtone of LO phonon at $q = 0$ measured from K point, (2) LO and TO combination phonon mode, at $q = 0$ measured from K point, (3) TO and LA combination phonon modes at $q = 2k$ measured from K point, and (4) overtone of iTO phonon at $q = 0$ measured from K point. The definition of $q = 0$ and $q = 2k$ will be given in Chapter 4. In this master thesis, we will calculate Raman spectra of G* band based on the all possibilities, and we will conclude the G* band process.

G$'$ band process is intervalley second-order Raman process. Phonon which contributing to G$'$ band is overtone of iTO phonon with phonon wave vector $q = 2k$ measured from K point.

Chapter 3

Basics properties of graphene

Basic physical properties of graphene is reviewed in this chapter. The geometrical structure, electronic properties and vibrational properties of graphene will be discussed in this chapter. The electronic structures is derived by simple and extended tight-tight binding approximation. The vibrational structure is obtained from force constant model up to the twentieth nearest neighbors.

3.1 Geometrical structure of graphene

Graphene is a two-dimensional (2D) material of carbon in a honeycomb lattice. In Fig.3.1 (a) we show the unit cell of graphene. The nearest-neighbor distance of two carboms of graphene is 1.42 Å (a_{cc}). Lattice vectors a_1 and a_2 are defined as

$$\begin{cases} \mathbf{a}_1 = \dfrac{\sqrt{3}a}{2}\hat{\mathbf{x}} + \dfrac{a}{2}\hat{\mathbf{y}}, \\ \mathbf{a}_2 = \dfrac{\sqrt{3}a}{2}\hat{\mathbf{x}} - \dfrac{a}{2}\hat{\mathbf{y}}, \end{cases} \tag{3.1}$$

where $a = \sqrt{3}\, a_{\mathrm{cc}} = 2.46$ Å is the lattice constant of graphene layer. $\hat{\mathrm{x}}$ and $\hat{\mathrm{y}}$ are the unit vectors in x and y directions of graphene layer, respectively as

---

Fig. 3.1: picuse/unit.eps

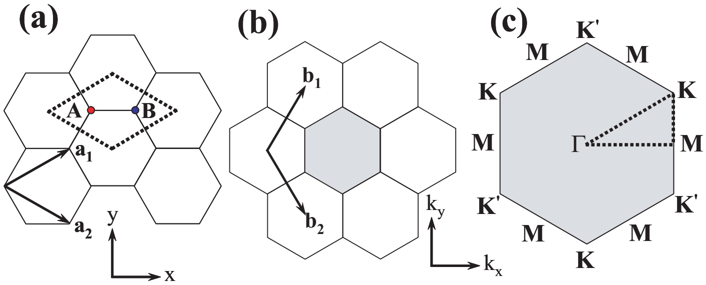

Figure 3.1 (a) The unit cell of graphene is shown as the dotted rhombus. The red and blue dots in the dotted rhombus represent the A and B sublattices, respectively. The unit vectors a_1 and a_2 are shown by arrows in the x, y coordinates system. (b) The first Brillouin zone is represented by a shaded region. The reciprocal lattice vectors b_1 and b_2 are shown by arrows in the k_x, k_y coordinates. (c) The first Brillouin zone of (b) labels Γ, K, K', and M indicate the high symmetry points. In general, energy dispersion relations are plotted along the edge of the dotted triangle connecting the high symmetry points, Γ, K and M [30].

shown in Fig. 3.1(a). The angle between two unit vectors $\mathbf{a_1}$ and $\mathbf{a_2}$ is 60°. The unit cell consists of two distinct carbon atoms A and B, respectively, by red and blue dots in Fig. 3.1 (a).

The reciprocal lattice vectors $\mathbf{b}_j$, $(j = 1, 2)$ are related to the real space vectors $\mathbf{a}_1$ and $\mathbf{a}_2$ according to the following definition:

$$\mathbf{a}_i \cdot \mathbf{b}_j = 2\pi\delta_{ij}, \tag{3.2}$$

where δ_{ij} is the Kronecker delta. The reciprocal unit vectors b_1 and b_2 are given by:

$$\begin{cases} \mathbf{b}_1 = \dfrac{2\pi}{\sqrt{3}a}\hat{\mathbf{x}} + \dfrac{2\pi}{a}\hat{\mathbf{y}}, \\ \mathbf{b}_2 = \dfrac{2\pi}{\sqrt{3}a}\hat{\mathbf{x}} - \dfrac{2\pi}{a}\hat{\mathbf{y}}, \end{cases} \tag{3.3}$$

where the size of angle between unit vectors $\mathbf{b}_1$ and $\mathbf{b}_2$ is 120° in Fig. 3.1 (b). In the Brillouin zone as shown in Fig. 3.1 (c), Γ (center), K, K',(corners of hexagonal) and M (center of edges) denote the high symmetry points.

3.2 Electronic structure

We review the simple tight-binding (STB) model which has important role to understand the electronic structure of graphene. In order to get the better result which agree with experimental result, we need to extend STB model by including the long-range atomic interaction and the σ molecular orbitals, and by optimizing the geometrical structure. This extends process is called extended tight-binding (ETB) method.

Carbon is the sixth element of the periodic table. A carbon atom has six electrons, denoted by $1s^2 2s^2 2p^2$; two electrons fill the inner shell $1s$ and four electrons occupy in the outer shell of $2s$ and $2p$ ($2p_x, 2p_y$, and $2p_z$) orbitals. In graphene, the π electrons in the $2p_z$ orbital are valence electrons which are contribute to the transport and other optical properties. The π electron has energy band structure around the Fermi energy, as a consequence electrons can be optically excited by visible or UV light from the valence band (π) to conduction band (π^*). We can obtain the electronic energy dispersion relations that consists $2s$ and $2p$ of graphene by solving the Scrödinger equation :

$$\hat{H}\Psi^b(k,r,t) = i\hbar\frac{\partial}{\partial t}\Psi^b(k,r,t), \tag{3.4}$$

where $\hat{H}$, the single-particle Hamiltonian operator is given by the following expression:

$$\hat{H} = -\frac{\hbar^2}{2m}\nabla^2 + U(r), \tag{3.5}$$

where ∇, $\hbar$, m, $U(r)$ and $\Psi^b(k,r,t)$, respectively, denote the gradient operator, the Planck's constant, the electron mass, the effective periodic potential, and one electron wave function. b $(= 1, 2, ..., 8)$ is the electron energy band index, k is the electron wave vector, r is the spatial coordinate, and t is time. The one electron wave function $\Psi^b(k,r,t)$ is constructed from four atomic orbitals, $2s$, $2p_x$, $2p_y$, and $2p_z$, for two inequivalent carbon atoms at the sublattice A and B as shown in Fig. 3.1(a). The one electron wave function is approximated by a linear combination of atomic orbitals (LCAO) in the term of Bloch wave function [31]:

$$\Psi^b(k,r,t) = e^{iE^b(k)t/\hbar} \sum_{s}^{A,B} \sum_{o}^{2s,\ldots,2p_z} C^b_{so}(k)\Phi_{so}(k,r), \tag{3.6}$$

where $E^b(k)$ and C^b_{so} are respectively the one electron energy, and the wave function coefficient for the Bloch function $\Phi_{so}(k,r)$. The Bloch wave function $\Phi_{so}(k,r)$ is given by a sum over the atomic wave function $\phi_o(r)$ for each atomic orbital of a sublattice A or B at the u-th unit cell in a graphene:

$$\Phi_{so}(k,r) = \frac{1}{\sqrt{U}} \sum_{u}^{U} e^{ik\cdot R_{us}} \phi_o(r - R_{us}), \tag{3.7}$$

where the index u $(= 1,...,U)$ represent summation of all the U unit cells in graphene and R_{us} is the atomic coordinate for the $u-$th unit cell and $s-$th atom. The electron wave function $\Psi^b(k,r,t)$ should satisfy the Bloch's theorem, as a consequence the summation in Eq. (3.6) should taken only for the Bloch wave function $\Phi_{so}(k,r)$ with the same value of k. The energy (eigen value) $E^b(k)$ as a function of k is given by:

$$E^b(k) = \frac{\langle \Psi(k)|\hat{H}|\Psi(k)\rangle}{\langle \Psi(k)|\Psi(k)\rangle}. \tag{3.8}$$

Substituting Eq. (3.6) into Eq. (3.8), we can obtain the following equation :

$$E^b(k) = \frac{\displaystyle\sum_{s'o'}\sum_{so} C^{b^*}_{s'o'}(k) H_{s'o'so}(k) C^b_{so}(k)}{\displaystyle\sum_{s'o'}\sum_{so} C^{b^*}_{s'o'}(k) S_{s'o'so}(k) C^b_{so}(k)}. \tag{3.9}$$

The transfer integral $H_{s'o'so}(k)$ and overlap integral $S_{s'o'so}(k)$ matrices are defined by:

$$\begin{aligned} H_{s'o'so}(k) &= \frac{1}{U}\sum_{u}^{U} e^{ik\cdot(R_{us}-R_{u's'})} \int \phi^*_{o'}(r - R_{u's'}) H \phi_o(r - R_{us}) dr, \\ S_{s'o'so}(k) &= \frac{1}{U}\sum_{u}^{U} e^{ik\cdot(R_{us}-R_{u's'})} \int \phi^*_{o'}(r - R_{u's'}) \phi_o(r - R_{us}) dr. \end{aligned} \tag{3.10}$$

The wave function coefficient $C^{b^*}_{s'o'}(k)$ should be optimized so as to minimize $E^b(k)$. The coefficient $C^{b^*}_{s'o'}(k)$ as a function of k is a complex variable and both $C^{b^*}_{s'o'}(k)$ and $C^b_{so}(k)$ are independent each other. In order to get the variational condition for finding the minimum of the ground state energy [30] :

$$\frac{\partial E^b(k)}{\partial C^{b*}_{s'o'}(k)} = 0. \tag{3.11}$$

By substituting the ground state energy $E^b(k)$ from Eq. (3.8) into Eq. (3.11), Eq. (3.11) we can obtain:

$$\begin{aligned}
\frac{\partial E^b(k)}{\partial C^{b*}_{s'o'}(k)} &= \frac{\sum\limits_{so} H_{s'o'so}(k) C^b_{so}(k)}{\sum\limits_{s'o'}\sum\limits_{so} C^{b^*}_{s'o'}(k) S_{s'o'so}(k) C^b_{so}(k)} \\
&\quad - \frac{\sum\limits_{s'o'}\sum\limits_{so} C^{b^*}_{s'o'}(k) H_{s'o'so}(k) C^b_{so}(k)}{\Big(\sum\limits_{s'o'}\sum\limits_{so} C^{b^*}_{s'o'}(k) S_{s'o'so}(k) C^b_{so}(k)\Big)^2} \sum_{so} S_{s'o'so}(k) C^b_{so}(k) \\
&= \frac{\sum\limits_{so} H_{s'o'so}(k) C^b_{so}(k) - E^b(k) \sum\limits_{so} S_{s'o'so}(k) C^b_{so}(k)}{\sum\limits_{s'o'}\sum\limits_{so} C^{b^*}_{s'o'}(k) S_{s'o'so}(k) C^b_{so}(k)} \\
&= 0.
\end{aligned} \tag{3.12}$$

By multiplying both side of eq. (3.12) with $\sum\limits_{s'o'}\sum\limits_{so} C^{b^*}_{s'o'}(k) S_{s'o'so}(k) C^b_{so}(k)$, (3.12) becomes more simple :

$$\sum_{so} H_{s'o'so}(k) C^b_{so}(k) - E^b(k) \sum_{so} S_{s'o'so}(k) C^b_{so}(k) = 0. \tag{3.13}$$

Eq. (3.13) is expressed in the matrix form when we define the $C^b_{so}(k)$ as a column vector, then we can get :

$$\begin{gathered}
C^b(k) = \begin{pmatrix} C^b_{2s^A} \\ \vdots \\ C^b_{2p_z^B} \end{pmatrix}, (b = 1, \cdots, 8). \\
\Big(H(k) - E^b(k) S(k)\Big) C^b(k) = 0,
\end{gathered} \tag{3.14}$$

The eigenvalues are calculated by solving the secular equation for given k:

$$\det\Big[H(k) - E^b(k)S(k)\Big] = 0. \tag{3.15}$$

The solution of (3.15) gives eight eigenvalues for the energy band index $b = 1, \cdots, 8$ for a given electron wave vector k. By considering only four atomic orbitals for each atom carbon $(2s, 2p_x, 2p_y, 2p_z)$ and there are two carbon atomic sites (A, B) per unit cell of a graphene, we can obtain the 8×8 Hamiltonian $H_{s'o'so}(k)$ and overlap $S_{s'o'so}(k)$ matrices. These matrices can be expressed by 2×2 sub-matrix for two sub-atoms:

$$H(k) = \begin{pmatrix} H_{AA}(k) & H_{AB}(k) \\ H_{BA}(k) & H_{BB}(k) \end{pmatrix} \text{ and } S(k) = \begin{pmatrix} S_{AA}(k) & S_{AB}(k) \\ S_{BA}(k) & S_{BB}(k) \end{pmatrix}, \tag{3.16}$$

where H_{AA} (H_{BB}) and H_{AB} (H_{BA}) are expressed by 4×4 sub-matrix for four orbitals $(2s, 2p_x, 2p_y, 2p_z)$. The matrix elements between $2p_z$ orbital and $2s$, $2p_x$, and $2p_y$ are zero because of the odd (even) function $2p_z$ ($2s$,

$2p_x$, and $2p_y$) of z for the both cases of H_{AA} (H_{BB}) and H_{AB} (H_{BA}):

$$\begin{aligned}
H_{AA}(k) &= \begin{pmatrix}
\langle 2s^A|H|2s^A\rangle & \langle 2s^A|H|2p_x^A\rangle & \langle 2s^A|H|2p_y^A\rangle & \langle 2s^A|H|2p_z^A\rangle \\
\langle 2p_x^A|H|2s^A\rangle & \langle 2p_x^A|H|2p_x^A\rangle & \langle 2p_x^A|H|2p_y^A\rangle & \langle 2p_x^A|H|2p_z^A\rangle \\
\langle 2p_y^A|H|2s^A\rangle & \langle 2p_y^A|H|2p_x^A\rangle & \langle 2p_y^A|H|2p_y^A\rangle & \langle 2p_y^A|H|2p_z^A\rangle \\
\langle 2p_z^A|H|2s^A\rangle & \langle 2p_z^A|H|2p_x^A\rangle & \langle 2p_z^A|H|2p_y^A\rangle & \langle 2p_z^A|H|2p_z^A\rangle
\end{pmatrix} \\
&= \begin{pmatrix}
\langle 2s^A|H|2s^A\rangle & 0 & 0 & 0 \\
0 & \langle 2p_x^A|H|2p_x^A\rangle & 0 & 0 \\
0 & 0 & \langle 2p_y^A|H|2p_y^A\rangle & 0 \\
0 & 0 & 0 & \langle 2p_z^A|H|2p_z^A\rangle
\end{pmatrix} \\
&= H_{BB}(k), \\
H_{AB}(k) &= \begin{pmatrix}
\langle 2s^A|H|2s^B\rangle & \langle 2s^A|H|2p_x^B\rangle & \langle 2s^A|H|2p_y^B\rangle & \langle 2s^A|H|2p_z^B\rangle \\
\langle 2p_x^A|H|2s^B\rangle & \langle 2p_x^A|H|2p_x^B\rangle & \langle 2p_x^A|H|2p_y^B\rangle & \langle 2p_x^A|H|2p_z^B\rangle \\
\langle 2p_y^A|H|2s^A\rangle & \langle 2p_y^A|H|2p_x^A\rangle & \langle 2p_y^A|H|2p_y^B\rangle & \langle 2p_y^A|H|2p_z^B\rangle \\
\langle 2p_z^A|H|2s^A\rangle & \langle 2p_z^A|H|2p_x^B\rangle & \langle 2p_z^A|H|2p_y^B\rangle & \langle 2p_z^A|H|2p_z^B\rangle
\end{pmatrix} \\
&= \begin{pmatrix}
\langle 2s^A|H|2s^B\rangle & \langle 2s^A|H|2p_x^B\rangle & \langle 2s^A|H|2p_y^B\rangle & 0 \\
\langle 2p_x^A|H|2s^B\rangle & \langle 2p_x^A|H|2p_x^B\rangle & \langle 2p_x^A|H|2p_y^B\rangle & 0 \\
\langle 2p_y^A|H|2s^A\rangle & \langle 2p_y^A|H|2p_x^A\rangle & \langle 2p_y^A|H|2p_y^B\rangle & 0 \\
0 & 0 & 0 & \langle 2p_z^A|H|2p_z^B\rangle
\end{pmatrix} \\
&= {}^{T}H_{BA}^{*}(k).
\end{aligned} \tag{3.17}$$

Because the atomic orbital $2s$, $2p_x$, and $2p_z$ are even function of z, which parallel to the graphene layer, and $2p_z$ is an odd function of z, these matrices can be partitioned into the 6×6 and 2×2 sub-matrices corresponding to the σ and π orbitals in the graphene case. In the case of simple tight-binding (STB) Model, the σ molecular orbitals and the long-range atomic interactions in the π bonding for $R > a_{CC}$ are neglected. Thus in the STB, we only solve a 2×2 sub-matrix to obtain the energy dispersion relation $E^B(k)$. We consider only nearest-neighbor interactions only, and the integration over a single atom in $H_{AA}(k)$ and $H_{BB}(k)$: The matrix Hamiltonian is given by :

$$\begin{aligned} H_{AA}(k) &= \frac{1}{U}\sum_{u}^{U} e^{ik\cdot(R_{uA}-R_{u'A})}\int \phi_\pi^*(r-R_{u'A})H\phi_\pi(r-R_{uA})dr \\ &= \frac{1}{U}\sum_{u=u'}^{U}\varepsilon_{2p} + \frac{1}{U}\sum_{R_{uA}=R_{u'A}\pm a}^{U} e^{\pm ika}\int \phi_\pi^*(r-R_{u'A})H\phi_\pi(r-R_{uA})dr \\ &\quad +(\text{terms equal to or more distance than } R_{uA}=R_{u'A}\pm 2a) \\ &= \varepsilon_{2p} + (\text{terms equal to or more distance than } R_{uA}=R_{u'A}\pm a). \end{aligned} \tag{3.18}$$

The maximum contribution to the matrix element $H_{AA}(k)$ comes from $u = u'$, as a consequence it gives the orbital energy of the $2p$ level, ε_{2p}. For simplicity in this calculation the next order is neglected . The absence of nearest-neighbor interactions within the same unit cell atom A or B yields the diagonal Hamiltonian and overlap matrix elements, $H_{AA}(k) = H_{BB}(k) = \varepsilon_{2p}$ and $S_{AA}(k) = S_{BB}(k) = 1$. For the $H_{AB}(k)$ and the $S_{AB}(k)$ matrix elements, the inter-atomic vectors R_A^n from A atom site to its three nearest-neighbor B atoms ($n = 1, 2, 3$) in Eq. (3.10) are given as follows (see Fig. 3.2):

$$\begin{aligned} &r_A^1 = (\frac{1}{\sqrt{3}}, 0)a, \quad r_A^2 = (-\frac{1}{2\sqrt{3}}, \frac{1}{2})a, \quad r_A^3 = (-\frac{1}{2\sqrt{3}}, -\frac{1}{2})a, \\ &r_B^1 = (-\frac{1}{\sqrt{3}}, 0)a, \quad r_B^2 = (\frac{1}{2\sqrt{3}}, -\frac{1}{2})a, \quad r_B^3 = (\frac{1}{2\sqrt{3}}, \frac{1}{2})a, \end{aligned} \tag{3.19}$$

where a is the lattice constant of graphene. According to the geometry of graphene, $r_A^n = -r_B^n$. By substituting (3.19) into (3.10), we can obtain

---

Fig. 3.2: picuse/vectorconecting.eps

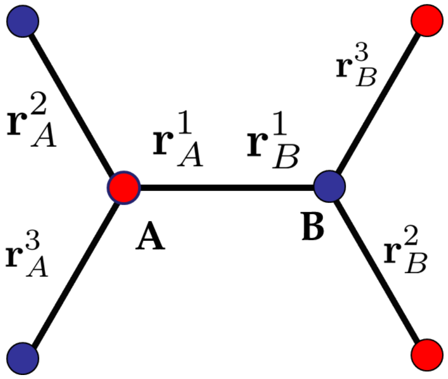

Figure 3.2 Vectors connecting nearest neighbor atoms in graphene for A and B atoms. The vectors are given in Eq. (3.19).

the matrix elements:

$$\begin{aligned}
H_{AB}(k) &= \frac{1}{U}\sum_{u}^{U} e^{ik\cdot(R_{uB}-R_{u'A})}\int \phi_\pi^*(r-R_{u'A})H\phi_\pi(r-R_{uB})dr \\
&= t\sum_{n}^{3} e^{ik\cdot R_A^n} \\
&= tf(k), \\
S_{AB}(k) &= \frac{1}{U}\sum_{u}^{U} e^{ik\cdot(R_{uB}-R_{u'A})}\int \phi_\pi^*(r-R_{u'A})\phi_\pi(r-R_{uB})dr \\
&= s\sum_{n}^{3} e^{ik\cdot R_A^n} \\
&= sf(k),
\end{aligned} \tag{3.20}$$

where t and s respectively are transfer integral and overlap integral between the nearest-neighbor A and B atoms. $f(k)$ is defined by starting from an A atom to the three nearest-neighbor B atoms. t, s and $f(k)$ are given by :

$$\begin{aligned} t &= \int \phi_\pi^*(r - R_{u'A}) H \phi_\pi(r - R_{uB}) dr, \\ s &= \int \phi_\pi^*(r - R_{u'A}) \phi_\pi(r - R_{uB}) dr, \\ f(k) &= e^{ik_x a/\sqrt{3}} + 2e^{-ik_x a/2\sqrt{3}} \cos\Big(\frac{k_y a}{2}\Big). \end{aligned} \tag{3.21}$$

The $H_{BA}(k)$ and $S_{BA}(k)$ matrix elements are derived by similar method with inter-atomic vector r_B^n from B atom site to its three nearest-neighbor A atoms, that is, $H_{BA}(k) = tf^*(k)$, and $S_{BA}(k) = sf^*(k)$. The $H(k)$ and $S(k)$ are Hermite matrices. The secular equation Eq. (3.15) for $H(k)$ and $S(k)$ can be written as follows:

$$\begin{pmatrix} \varepsilon_{2p} & tf(k) \\ tf^*(k) & \varepsilon_{2p} \end{pmatrix} \begin{pmatrix} C^b_{A\pi}(k) \\ C^b_{B\pi}(k) \end{pmatrix} = E^b(k) \begin{pmatrix} 1 & sf(k) \\ sf^*(k) & 1 \end{pmatrix} \begin{pmatrix} C^b_{A\pi}(k) \\ C^b_{B\pi}(k) \end{pmatrix}. \tag{3.22}$$

The eigenvalues $E^b(k)$ are obtained by solving the secular equation in Eq. (3.15):

$$\begin{vmatrix} \varepsilon_{2p} - E^b(k) & f(k)\Big(t - sE^b(k)\Big) \\ f^*(k)\Big(t - sE^b(k)\Big) & \varepsilon_{2p} - E^b(k) \end{vmatrix} = 0, \tag{3.23}$$

Solving this secular equation yields the energy eigenvalue:

$$\begin{cases} E^v(k) = \dfrac{\varepsilon_{2p} + tw(k)}{1 + sw(k)}, \\ E^c(k) = \dfrac{\varepsilon_{2p} - tw(k)}{1 - sw(k)}, \end{cases} \tag{3.24}$$

where the band indexes $b = v, c$ denote the valence and conduction bands, $(t < 0)$, $(s > 0)$, and $w(k)$ is the absolute value of the phase factor $f(k)$, that is, $w(k) = \sqrt{f^*(k)f(k)}$:

$$w(k) = \sqrt{1 + 4\cos\Big(\frac{\sqrt{3}}{2}k_x a\Big)\cos\Big(\frac{1}{2}k_y a\Big) + 4\cos^2\Big(\frac{1}{2}k_y a\Big)}. \tag{3.25}$$

The overlap integral s is responsible for the asymmetry between the valence and conduction energy bands. When the overlap integral s becomes zero $(s = 0)$, the valence and conduction bands become symmetrical around

$E = \varepsilon_{2p}$ which can be understood from Eq. (3.24). By substituting the energy eigenvalues $E^b(k)$ of Eq. (3.24), the wave function coefficients $C_A^b(k)$ and $C_B^b(k)$ for the energy bands $b = v, c$ are yielded:

$$\begin{cases} \Big(\varepsilon_{2p} - E^b(k)\Big) C_A^b(k) + f(k)\Big(t - sE^b(k)\Big) C_B^b(k) = 0, \\ f^*(k)\Big(t - sE^b(k)\Big) C_A^b(k) + \Big(\varepsilon_{2p} - E^b(k)\Big) C_B^b(k) = 0, \end{cases}$$

therefore,

$$\begin{cases} C_A^v(k) = \dfrac{f(k)}{w(k)} C_B^v(k)\ ,\ C_B^v(k) = \dfrac{f^*(k)}{w(k)} C_A^v(k), \\ C_A^c(k) = -\dfrac{f(k)}{w(k)} C_A^c(k)\ ,\ C_B^c(k) = -\dfrac{f^*(k)}{w(k)} C_A^c(k). \end{cases} \tag{3.26}$$

The orthonormal conditions for the electron wave function of Eq. (3.6) can be expanded in terms of Bloch wave functions:

$$\begin{aligned} &\langle \Psi^{b'}(k, r, t) | \Psi^b(k, r, t) \rangle \\ &= \sum_{s'}^{A,B} \sum_{s}^{A,B} C_{s'}^{b'^*}(k) C_s^b(k) S_{s's}(k) \\ &= C_A^{b'^*}(k) C_A^b(k) + s f(k) C_A^{b'^*}(k) C_B^b(k) + s f^*(k) C_B^{b'^*}(k) C_A^b(k) + C_B^{b'^*}(k) C_B^b(k) \\ &= \delta_{b'b},\ (b', b = v, c). \end{aligned} \tag{3.27}$$

Thus, we obtain the wave function coefficients $C_A^b(k)$ and $C_B^b(k)$ for π electrons which are related to each other by complex conjugation, for the valence band $b = v$,

$$C_A^v(k) = \sqrt{\frac{f(k)}{2w(k)(1 + sw(k))}}\ ,\ C_B^v(k) = \sqrt{\frac{f^*(k)}{2w(k)(1 + sw(k))}}, \tag{3.28}$$

for the conduction band $b = c$,

$$C_A^c(k) = \sqrt{\frac{f(k)}{2w(k)(1 - sw(k))}}\ ,\ C_B^c(k) = -\sqrt{\frac{f^*(k)}{2w(k)(1 - sw(k))}}. \tag{3.29}$$

The STB method is simple method and give good agreement with the first principle calculation if the value of transfer integral $t = -3.033$ eV, overlap integral $s = 0.129$eV [30].

Table 3.1: Tight binding parameters of graphene obtained from a fit to first principles calculations [30]. ϵ_{2s} is defined relative to the setting $\epsilon_{2p} = 0$.

bond	H	value (eV)	S	value
ssσ	H_{2s2s}	-6.769	S_{2s2s}	0.212
spσ	H_{2s2p}	-5.580	S_{2s2p}	0.102
ppσ	$H_{\mathrm{pp}\sigma}$	-5.037	$S_{\mathrm{pp}\sigma}$	0.146
ppπ	$H_{\mathrm{pp}\pi} = t$	-3.033	$S_{\mathrm{pp}\pi} = s$	0.129
	ϵ_{2s}	-8.868		

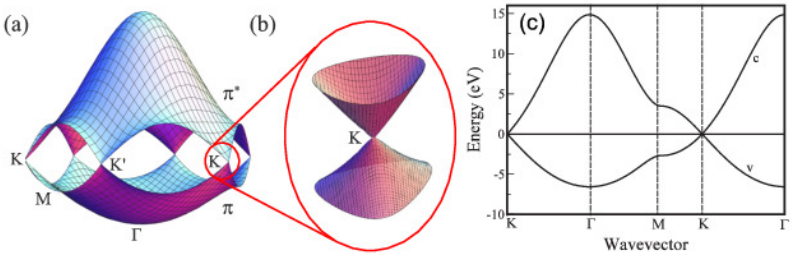

Figure 3.3 Energy dispersion relations of a graphene for π bands given by Eq. (3.24), transfer integral $t = -3.033$ eV, overlap integral $s = 0.129$ eV, and atomic orbital energy $\varepsilon_{2p} = 0$ eV, (a) 3D figure for the whole region of the Brillouin zone, (b) near the K point, the energy dispersion shows the linear disperison (c) along the high symmetry direction of $K - \Gamma - M - K - \Gamma$ (Fig. 3.1), the valence and conduction bands are denoted by v and c, respectively[30].

In the case of the extended tight-binding (ETB), we need to solve the equation in Eq. (3.17). The matrix elements in Eq. (3.17) are given by Eq. (3.30). The numerical values of H_{so} and S_{so} in Eq.(3.30) are listed in Table 3.1. We solve the Eq. (3.15) and plot the energy dispersion as shown in Fig. 3.4. If we use simple tight-binding (STB), we just obtain π and $\pi^\star$ bands as shown in Fig.3.3, but by using extended tight binding we can obtain eight

---

Fig. 3.3: picuse/dispersion.eps

bands, such as σ_{SS}, π, $\sigma_{PP}+\pi^\star$, $\pi^\star$, $\sigma^\star_{PP}+\pi$ and $\sigma^\star_{SS}$.

$$\begin{aligned}
\langle 2\mathrm{s}^{\mathrm{A}}|H|2\mathrm{s}^{\mathrm{B}}\rangle &= H_{2\mathrm{s}2\mathrm{s}}(p_1+p_2+p_3)\\
\langle 2\mathrm{p}_x^{\mathrm{A}}|H|2\mathrm{s}^{\mathrm{B}}\rangle &= H_{2\mathrm{s}2\mathrm{p}}\left(p_1-\frac{p_2}{2}-\frac{p_3}{2}\right)\\
\langle 2\mathrm{p}_y^{\mathrm{A}}|H|2\mathrm{s}^{\mathrm{B}}\rangle &= \frac{\sqrt{3}}{2}H_{2\mathrm{s}2\mathrm{p}}\left(-p_2+p_3\right)\\
\\
\langle 2\mathrm{s}^{\mathrm{A}}|H|2\mathrm{p}_x^{\mathrm{B}}\rangle &= \frac{\sqrt{3}}{2}H_{2\mathrm{s}2\mathrm{p}}(-p_1+\frac{p_2+p_3}{2})\\
\langle 2\mathrm{p}_x^{\mathrm{A}}|H|2\mathrm{p}_x^{\mathrm{B}}\rangle &= H_\sigma\left(\frac{-p_1-p_2-p_3}{4}\right)+\frac{3}{4}H_\pi(p_2+p_3)\\
\langle 2\mathrm{p}_y^{\mathrm{A}}|H|2\mathrm{p}_x^{\mathrm{B}}\rangle &= \frac{\sqrt{3}}{4}\left(H_\sigma+H_\pi\right)\left(p_2-p_3\right) \qquad (3.30)\\
\\
\langle 2\mathrm{s}^{\mathrm{A}}|H|2\mathrm{p}_y^{\mathrm{B}}\rangle &= \frac{\sqrt{3}}{2}H_{2\mathrm{s}2\mathrm{p}}(-p_2+p_3)\\
\langle 2\mathrm{p}_x^{\mathrm{A}}|H|2\mathrm{p}_y^{\mathrm{B}}\rangle &= \frac{\sqrt{3}}{4}\left(H_\sigma+H_\pi\right)\left(p_2-p_3\right)\\
\langle 2\mathrm{p}_y^{\mathrm{A}}|H|2\mathrm{p}_y^{\mathrm{B}}\rangle &= -\frac{3}{4}H_\sigma(p_2+p_3)+H_\pi\left(p_1+\frac{p_2+p_3}{4}\right)\\
\\
\langle 2\mathrm{p}_z^{\mathrm{A}}|H|2\mathrm{p}_z^{\mathrm{B}}\rangle &= H_\pi\left(p_1+p_2+p_3\right).
\end{aligned}$$

For the on–site elements in H_{AA} and H_{BB}, we define

$$\langle 2s^{\mathrm{A}}|H|2s^{\mathrm{A}}\rangle = \langle 2s^{\mathrm{B}}|H|2s^{\mathrm{B}}\rangle = \epsilon_s, \quad \langle 2p^{\mathrm{A}}|H|2p^{\mathrm{A}}\rangle = \langle 2p^{\mathrm{B}}|H|2p^{\mathrm{B}}\rangle = 0. \qquad (3.31)$$

Unlike the most ordinary semiconductors, the energy band structure of graphene shows the linear **k** dependence around the K and K' points near the Fermi level ($E=0$), as can be seen in Fig. 3.3. The energy dispersion of graphene also shows graphene does not has an energy gap between the valence and conduction bands, but the valence and conduction bands do not overlap each other. Around the K point in the first Brillouin zone, the electron wave vector k is written to the form $k_x = \Delta k_x$ and $k_y = -4\pi/(3a)+\Delta k_y$, where $\Delta k_x, \Delta k_y \ll 1/a$. Substituting these wave vectors into Eq. (3.25) and approximating the cosine function up to the second order

---

Fig. 3.4: picuse/sigma-band.eps

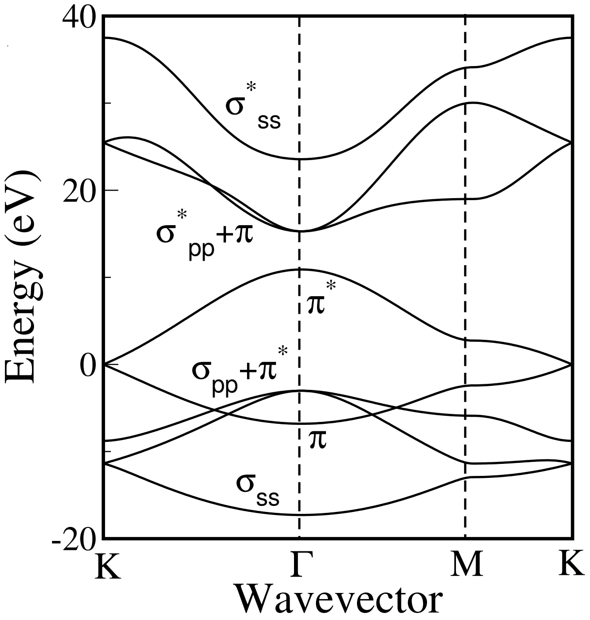

Figure 3.4 The σ and π bands of graphene within extended tight-binding method along the $K-\Gamma-M-K$ direction. In K point π and $\pi^\star$ bands, touch each other.

in the Maclaurin series as functions of $\Delta k_x a$ and $\Delta k_y a$, we can obtain w as a function of Δk (distance from the K point),

$$\begin{aligned} w(k) &= \sqrt{1+4\cos\Big(\frac{\sqrt{3}}{2}\Delta k_x a\Big)\cos\Big(-\frac{2}{3}\pi+\frac{1}{2}\Delta k_y a\Big)+4\cos^2\Big(-\frac{2}{3}\pi+\frac{1}{2}\Delta k_y a\Big)} \\ &\approx \frac{\sqrt{3}}{2}\Delta k a, \ \Big(\Delta k=\sqrt{\Delta k_x^2+\Delta k_y^2}\ ,\ \cos x = 1-\frac{x^2}{2!}+\frac{x^4}{4!}-\frac{x^6}{6!}+\cdots\Big), \end{aligned} \tag{3.32}$$

and then the energy dispersion relations for the valence and conduction bands are yielded by substituting w into Eq. (3.24):

$$\begin{cases} E^v(\Delta k) = \varepsilon_{2p} - \dfrac{\sqrt{3}}{2}(\varepsilon_{2p}s - t)a\Delta k, \\ \\ E^c(\Delta k) = \varepsilon_{2p} + \dfrac{\sqrt{3}}{2}(\varepsilon_{2p}s - t)a\Delta k. \end{cases} \tag{3.33}$$

Eq. (3.33) shows that the energy band for the valence and conduction band are linear in Δk.

3.3 Phonon energy dispersion

Phonon energy dispersion are important information to study vibrational phenomena. From the phonon energy dispersion, we can get some information, such as mechanical, thermal, and other condensed matter phenomena [32]. We calculate the phonon energy dispersion by using the force constant model up to the twentieth nearest neighbors. In the unit cell of graphene consist of two atoms, A and B atoms, there are six branches in the phonon dispersion relations. They are out-of-plane transverse acoustic (oTA), in-plane transverse acoustic (iTA), longitudinal acoustic (LA), out-of-plane transverse optic (oTO), in-plane transverse optic (iTO) and longitudinal optic (LO) as shown in Fig. 3.5. Three of them (LA, iTA, and oTA) are acoustic modes because of the three freedom degree in x, y and z axis. The others three (LO, iTO, and oTO) are optical branch.

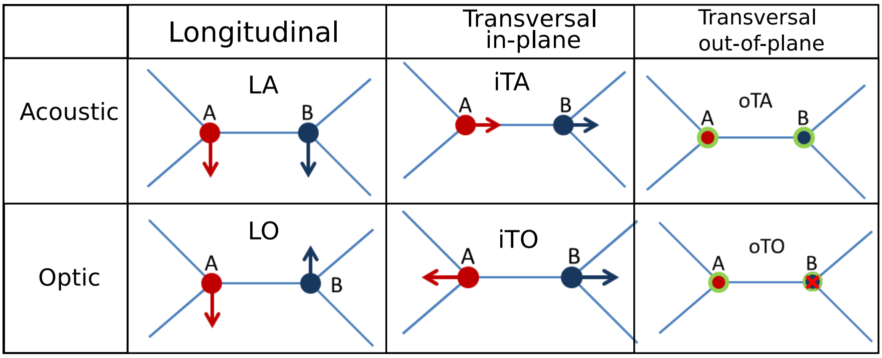

Figure 3.5 Illustration of the atomic vibration in unit cell of monolayer graphene. There are six phonon branches.

The phonon dispersion relations are calculated using a force constant model, in which the i–th atom is connected to its j–th neighbor atom through a force constant tensor $K^{(ij)}$. The components of the force constant tensors are made from the force constants. Since the force between two atoms decreases with increasing inter–atomic distance, interactions can be neglected

---

Fig. 3.5: picuse/phononbranch.eps

for a longer distance than the cut–off radius. The equation of motion for the displacement of the i–th atom, measured from the equivalent position $\mathbf{u}_i = (x_i, y_i, z_i)$ for N atom in unit cell is given by

$$M_i \ddot{\mathbf{u}}_i = \sum_j K^{(ij)}(\mathbf{u}_j - \mathbf{u}_i), \quad (i = 1, \cdots, N), \tag{3.34}$$

Where M_i and $K^{(ij)}$ respectively represent mass of the i–th atom and 3×3 force constant tensor between i–th and j–th atoms. The summation over j is taken over the twentieth nearest neighbor atoms [33, 34]. Now we can perform the Fourier transform of the displacement of the i–th atom with the wave number $\mathbf{q}$ to obtain the normal mode displacement $\mathbf{u_i}(k)$

$$\mathbf{u}_i(k) = \frac{1}{\sqrt{N_\Omega}} \sum_{q'} e^{-i(q' \cdot R_i - \omega t)\mathbf{u}'_q}, \quad \mathbf{u}_q(k) = \frac{1}{\sqrt{N_\Omega}} \sum_{R_i} e^{-i(q \cdot R_i - \omega t)\mathbf{u}_i} \tag{3.35}$$

where N_σ is the number of unit cell in the solid, summation is taken over all wave vector $\mathbf{q}'$ in the first Brillouin zone. R_i denotes the atomic position of the ith atom in the crystal. We assume the same eigen frequencies ω for all $\mathbf{u}_i$. By substituting $\ddot{\mathbf{u}}_i(k) = -\omega(k)^2 u_i(k)$ to the equation of motion in Eq. (3.34) and by defining $3N \times 3N$ dynamical matrix $\mathcal{D}(\mathbf{q})$

$$\mathcal{D}(\mathbf{q})\mathbf{u}_q = 0. \tag{3.36}$$

In order to obtain the eigenvalues $\omega^2(\mathbf{q})$ for $\mathcal{D}(\mathbf{q})$ and non trivial condition $\mathbf{u}_q \neq 0$, we solve the secular equation det $D(q) = 0$ for given $\mathbf{q}$ vector. It is convenient to divide the dynamical matrix $\mathcal{D}(\mathbf{q})$ into small 3×3 matrices $\mathcal{D}^{(ij)}(q)$. The dynamical matrix $\mathcal{D}^{(ij)}(q)$ defined by

$$\mathcal{D} = \begin{pmatrix} D^{AA} & D^{AB} \\ D^{BA} & D^{BB} \end{pmatrix}, \tag{3.37}$$

Fig. 3.6: picuse/phonondisp.eps

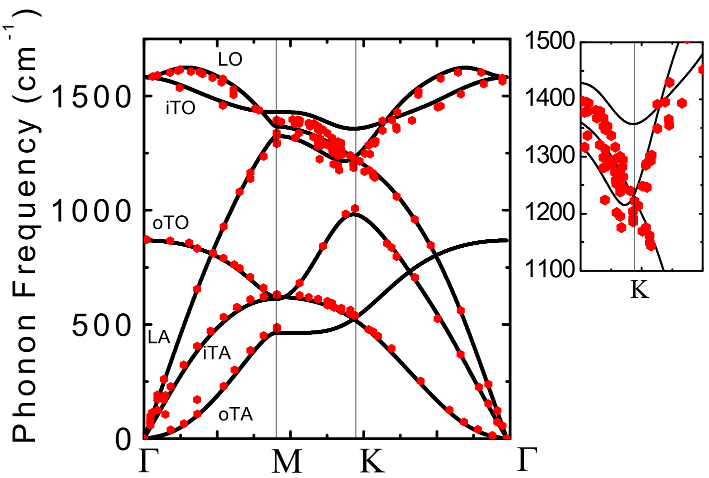

Figure 3.6 Phonon energy dispersion relation of graphene force constant model up to twentieth nearest neighbor atoms (black lines) fitted with experiment data of the X-ray inelastic scattering in graphene (red dots) by A. Grüneis *et al* [35], plotted along high symmetry direction. Inset shows the Phonon frequency near the K point.

with

$$\mathcal{D}^{(ij)}(q) = \left(\sum_{j''} K^{(ij'')} - M_i \omega^2(q) I \right) \delta_{ij} - \sum_{j'} K^{(ij')} e^{iq \cdot \Delta R_{ij'}}, \quad (i,j = A, B) \tag{3.38}$$

where the sum over j'' is taken over all neighbor sites from the i–th atom with $K^{(ij'')} \neq 0$, and the sum over j' is taken for the equivalent sites to the j–th atom. The first two terms of Eq. (3.38) have non-vanishing values only when $i = j$, and the last term appears only when the j–th atom is coupled to the i–th atom through $K^{(ij)} \neq 0$.

In a periodic system, the dynamical matrix elements are given by the product of the force constant tensor $K^{(ij)}$ and the phase difference factor $e^{ik \cdot \Delta R_{ij}}$, with ΔR_{ij} being the distance vector between atoms i and j. This situation is similar to the case of the tight binding calculation for the electronic structure where the matrix element is given by the product of the atomic matrix element and the phase difference factor.

Each shell has three different kinds force constants for in–plane radial r (along bond direction), in–plane transverse (t_i) (perpendicular to bond direction) and out–of–plane movements (To). Within a given shell, we put one atom on the x axis with coordinate of the radius of the shell. Then we can rotate the force constant tensor to any atom position on that shell by a rotation matrix U_m around the z axis perpendicular to the graphene plane. For the first shell U_m for the interaction of the type A atom with a B_m atom ($m = 1, 2, 3$) is given by [30]

$$U_m = \begin{pmatrix} \cos\theta_m & \sin\theta_m & 0 \\ -\sin\theta_m & \cos\theta_m & 0 \\ 0 & 0 & 1 \end{pmatrix}. \tag{3.39}$$

The force constant tensors in the first shell can be calculated using

$$K^{(A,Bm)} = U_m^{-1} K^{(A,B1)} U_m, \qquad (m = 2, 3). \tag{3.40}$$

For $m = 1$, U_m is the unity matrix and the force constant tensor has only diagonal elements and is given by

$$K^{(A,B1)} = \begin{pmatrix} \phi_r^{(1)} & 0 & 0 \\ 0 & \phi_{ti}^{(1)} & 0 \\ 0 & 0 & \phi_{to}^{(1)} \end{pmatrix}. \tag{3.41}$$

The force constant between an atom in the center and an atom on the positive x axis in the n–th shell shall be $\phi_r^{(n)}$ for in–plane radial, $\phi_{ti}^{(n)}$ for in–plane tangential and $\phi_{to}^{(n)}$ for out–of–plane plane vibrations.

The values of the force constant are obtained by fitting the 2D phonon dispersion relation over Brillouin zone as determined experimentally, as for an example from the energy loss spectroscopy and inelastic neutron scattering [33, 36].

In Fig. 3.6, we show the phonon energy dispersion curve for monolayer graphene were fitted to the experimental data of the x-ray inelastic scattering

[35]. We notice that the calculated phonon dispersion for the iTO branch which is the highest phonon energy near the K point, gives larger phonon energy around the K point than experimental results. However, all previous calculation show iTO phonon frequency near the K point is always higher than experiment [36, 37, 38]. The difference between experiment and theory might be come from failure of the adiabatic approximation, known as the Kohn-anomaly effect [7]. Since the iTO phonon dispersion near the K point is correspond to the G$'$ band and G* band, we will get higher calculated G$'$ and G* bands peak positions.

Chapter 4

Calculation method

In this chapter, we reviewed how to calculate Raman intensity of monolayer graphene graphene based on the first-order Raman process and the second-order Raman process. In order to calculate Raman intensity, we calculate electron-photon and electron-phonon matrix elements. So we also reviewed electron-photon and electron-phonon interactions, which was previously developed by Dr. J. Jiang [21], Dr. Jin Sun Park [39] and Dr. Alexander Grüneis [32] in our group.

4.1 Raman intensity calculation

We reviewed the Raman intensity calculation for first-order Raman process and for second-order Raman process. The G band Raman is first-order process. The G' and $\mathrm{G}^{\star}$ bands are the example of second-order Raman process. In order to calculate Raman intensity in Eq.(4.1) and Eq. (4.2), we need information about the phonon frequency. The phonon energy dispersion was calculated using force-constant tight binding model up to twentieth nearest neighbor, in which each atom is connected to its neighbor atom through a force constant tensor [33, 40] as explained in Section 3.3. Because there is a discrepancy near K point in the phonon energy dispersion, we also use

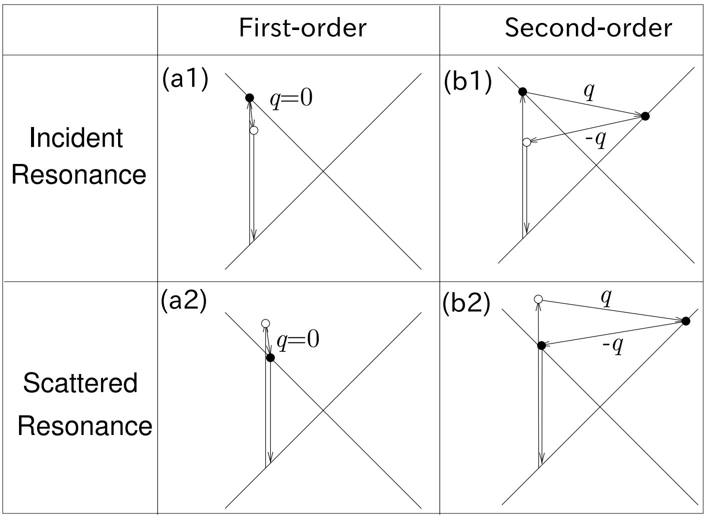

Figure 4.1 (a) One-phonon first-order Raman process, and (b) two-phonon second-order process. Resonance points are shown as solid circle [6].

Quantum Espresso to calculate the phonon energy dispersion. For simplicity we only consider electron-phonon scattering, and we neglect hole-phonon scattering process. According to the Raman intensity formula for first and second order processes [Eqs. (4.1) and (4.2)], the denominator corresponds to the peak positions and the numerator corresponds to intensity.

4.1.1 First-order resonance Raman spectroscopy

The order of Raman process is given by the number of inelastic scattering events that involved in the Raman process [26]. The first-order Raman process is the Raman process where the photon energy excitation creates one phonon in the crystal with very small momentum $q \approx 0$. Here the resonance means that the one (two) intermediate state is real electronic state (solid dots in Fig. 4.1) for the first (second) order process.

An electron with wave-vector $\mathbf{k}$ in an initial state i is excited by an

---

Fig. 4.1: picuse/ch3-srdr.eps.eps

incident photon with energy E_L from the i state to an excited m state by the absorption of an excitation energy $(E_m - E_i)$. If the m state is a real electronic state, the light absorption is the resonance process. This photoexcited electron will be further scattered by a $q \approx 0$ phonon with frequency ω_q to a virtual state m', and decay back to state i by emitting scattered light.

Therefore, the first-order Raman intensity as a function of E_L and phonon energy ω_q is given by third-order perturbation theory by [6, 26, 41, 42]

$$I(\omega_q, E_L) = \sum_i \left| \sum_{m,m'} \frac{M^{\mathrm{op}}(\mathbf{k\text{-}q}, im')M^{\mathrm{ep}}(\mathbf{q}, m'm)M^{\mathrm{op}}(\mathbf{k}, mi)}{(E_L - (E_m - E_i) + i\gamma_r)(E_L - \hbar\omega_q - (E'_m - E_i) + i\gamma_r)} \right|^2, \tag{4.1}$$

γ_r denotes the broadening factor of the resonance event. The broadening factor is related to the lifetime of the photoexcited electron in the excited states, that is the lifetime for Raman scattering process, which is the time delay between absorption of the incoming photon and emission of the outgoing photon. Particularly γ_r is the inverse of the lifetime for the photoexcited carrier [6]. The typical value of $\gamma_r = 0.1$ eV [26], which is independent of E_L for simplicity. However, when the E_L increases, the lifetime of photoexcited electron decreases, and the value of γ_r is expected to increase with increasing E_L [43, 44].

The physical process of first-order Raman is described by an electron at wave vector $\mathbf{k}$ that is (1) excited by an electric dipole interaction $M^{\mathrm{op}}(\mathbf{k}, mi)$ with the incident photon to make transition from i to m, then (2) the photoexcited electron is scattered from the m state to the m' state by emitting a phonon with frequency ω_q and wave-vector $\mathbf{q} = 0$ through an electron-phonon interaction, $M^{\mathrm{ep}}(\mathbf{q}, m'm)$, and finally (3) the photoexcited electron goes back from m' to the initial state i by emitting a photon, through the electron-photon interaction, $M^{\mathrm{op}}(\mathbf{k\text{-}q}, im')$. There are two possibilities for resonance condition $E_L = E_{mi}$ (incindent resonance) and $E_L = E_{mi} + \hbar\omega_q$

(scattered resonance) . The electron-photon and electron-phonon matrix elements will be discussed in Section 4.2 and 4.3.

In the case of Graphene, the degenerate LO and iTO phonon modes at Γ point are Raman active and they are related to the C-C bond stretching mode [3, 6, 26, 45, 46, 47]. LO and iTO modes at Γ point appear around 1580 cm^{-1} and contribute to the G band process. Thus the G band is the first-order Raman process.

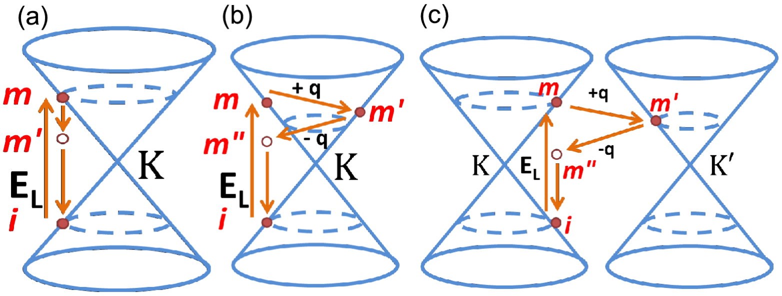

Figure 4.2 The Raman scattering process with laser excitation energy E_L, initial state i, excited state m, and intermediate states m' and m''. (a) One-phonon first-order Raman scattering process. Two-phonon second order resonant Raman processes (b) intravalley (c) intervalley.

4.1.2 Second-order Raman process

The Raman process which contributing two inelastic scattering events is called second-order Raman process. The story of second-order Raman process is almost the same with first-order Raman process, however, in the second-order Raman process we have two phonon scattering processes with phonon wave vector $\mathbf{q}$ and $-\mathbf{q}$. So that momentum conservation is possible for $q \neq 0$. There are two types of second-order Raman process, such as intravalley and intervalley processes as shown in Fig. 2.3(b) and (c).

However, The purpose of this section is to obtain formula for calculating Raman spectra of G′ and G⋆ band, as consequence we just discuss about

---

Fig. 4.2: picuse/firstandsecond.eps.eps

two-phonons second-order Raman process.

The second-order Raman intensity as a function of E_L and two phonons energy $\omega_1$and ω_2 is given by fourth-order perturbation theory by [6]

$$I(\omega_1+\omega_2,E_L) = \sum_i \left| \sum_{m,m',m'',\nu,\nu'} \frac{M^{\rm op}(\mathbf{k},im'')M^{\rm ep}(\text{-}\mathbf{q},m''m')}{(E_L-E_{mi}-i\gamma_r)(E_L-E_{m'i}-\hbar\omega_1^{\nu}-i\gamma_r)} \frac{M^{\rm ep}(\mathbf{q},m'm)M^{\rm op}(\mathbf{k},mi)}{(E_L-E_{m''i}-\hbar\omega_1^{\nu}-\hbar\omega_2^{\nu'}-i\gamma_r)}\right|^2, \tag{4.2}$$

in which

$$E_{mi} \equiv E_m - E_i. \tag{4.3}$$

In order to get two resonance conditions at the same time, an intermediate state is always in resonance condition ($E_L = E_{m'} - E_i + \hbar\omega_1$), and either the incident resonance condition ($E_L = E_m - E_i$) or scattered resonance ($E_L = E_{m''i} + \hbar\omega_1 + \hbar\omega_2$) is satisfied.

4.1.3 Double Resonance Raman Process

Double resonance Raman scattering consist of (1) two-phonon scattering processes and (2) one-phonon and one-elastic scattering processes [48]. Two phonon scattered can be the same phonon mode (an overtone mode) or different phonon modes (a combination phonon modes) [49, 50, 51].

Phonon wave vector $\mathbf{q}$ as shown in Fig. 4.3 is found by selecting an equi-energy contour with the same incident laser energy around the K point and another equi-energy contour around K' point after one phonon scattering. The double resonant Raman scattering process for the G' mode, as shown in Fig. 2.3(b) and (c), is given as follows: (i) an electron with a wave-vector $\mathbf{k}$ in an initial state i near the K point is excited by an incident photon from the i to m state by the electron-photon interaction, $M^{\rm op}(\mathbf{k},mi)$, then (ii) the photoexcited electron is scattered from m to m' to another valley K'

by emitting a phonon with frequency ω_1 and wave-vector $\mathbf{q}$ by the electron-phonon interaction, $M^{\mathrm{ep}}(\mathbf{q}, m'm)$, (iii) the photoexcited electron is scattered back from m' to m'' at the initial valley K by emitting a phonon with the electron-phonon interaction $M^{\mathrm{ep}}(\text{-}\mathbf{q}, m''m')$, and finally (iv) the electron at the m'' state recombines with a hole to the initial state i by emitting a photon by the electron-photon interaction, $M^{\mathrm{op}}(\mathbf{k}, im'')$. All possible final states for the phonon wave-vectors $\mathbf{q}$ of the double resonance Raman scattering processes are illustrated as the shaded region in Fig. 4.3.

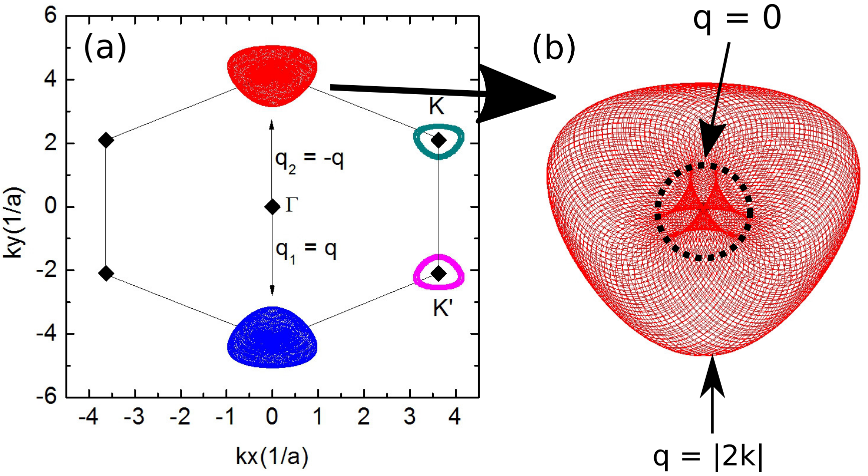

Figure 4.3 (a) Equi-energy contours for incident laser energy. Phonon wave vectors $\mathbf{q}$ from the Γ point, $\mathbf{q} = \mathbf{k}_f - \mathbf{k}_i$ (b) The collection of all possible phonon wave vectors, inside the black dashed circle for $q = 0$, and whole red lines for $q = 2k$.

In order to find the possibility of phonon wave vector as shown in Fig. 4.3, we select an equi-energy contour with the same incident laser excitation energy around the K point and another equi-energy contour around the K' point after one phonon scattering. For each point in K point, it has whole circle point intermediate state in the K' valley.

There are two conditions of phonon wave vector, $q = 0$ and $q = 2k$ as shown in Fig. 4.3(b). Where q is measured from the K point.

Fig. 4.3: picuse/qeq0.eps.eps

4.2 Electron-photon interactions

The electron-photon interaction for optical transition in solid consists of absorption and emission of photons. In the Raman spectra calculation, the electron-photon coupling is important, in order to calculate Raman intensity, we need to calculate the electron-photon matrix element.

4.2.1 Dipole approximation

The electron-photon interaction is obtained from time-dependent perturbation theory. The Hamiltonian for a charged particle with charge e and mass m in electromagnetic field is given by :

$$H = \frac{1}{2m}\left\{-i\hbar\nabla - e\mathbf{A}(t)\right\}^2 + V(\mathbf{r}), \tag{4.4}$$

where $\mathbf{A}(t)$, and $V(\mathbf{r})$ respectively represent vector potential and periodic crystal potential. We separated the Hamiltonian terms, unperturbed Hamiltonian $H_0 = -\frac{\hbar^2}{2m}\Delta + V(\mathbf{r})$ and perturbed Hamiltonian H_{opt}. For simplicity we neglect the quadratic term of $\mathbf{A}(t)$ in Eq. (4.4) and use the Coulomb gauge $\nabla \cdot \mathbf{A}(t) = 0$, The perturbation Hamiltonian of electron and causing its its transition from valence to conduction bands, vice versa are given by :

$$H_{\text{opt},\rho} = \frac{ie\hbar}{m}\mathbf{A}_\rho(t)\cdot\nabla \quad \text{with} \quad \rho = \text{A or E}. \tag{4.5}$$

The $\rho =$A, E denotes absorption or stimulated emission of light, respectively and determines the sign of $\pm i\omega t$ in the phase factors for electric and magnetic components of the wave. The Maxwell equation, which we need is in the SI units given as

$$\nabla \times \mathbf{B} = \epsilon_0\mu_0\frac{\partial \mathbf{E}}{\partial t}. \tag{4.6}$$

The electric that we used here is $\mathbf{E}_\rho(t) = \mathbf{E}_0\exp[i(\mathbf{k}\cdot\mathbf{r} \pm \omega t)]$ and magnetic fields is $\mathbf{B}_\rho(t) = \mathbf{B}_0\exp[i(\mathbf{k}\cdot\mathbf{r} \pm \omega t)]$. Thus $\mathbf{B} = \nabla \times \mathbf{A} = i\mathbf{k} \times \mathbf{A}$ and $\nabla \times \mathbf{B} = i\mathbf{k} \times \mathbf{B}$. By using $(\mathbf{A}\times\mathbf{B})\times\mathbf{C} = (\mathbf{A}\cdot\mathbf{C})\mathbf{B} - (\mathbf{B}\cdot\mathbf{C})\mathbf{A}$, we can write :

$$\nabla \times \mathbf{B} = k^2\mathbf{A} = \frac{1}{c^2}\frac{\partial \mathbf{E}}{\partial t}. \tag{4.7}$$

Since $\mathbf{E}$ is a plane wave, we get $\partial\mathbf{E}/\partial t = -i\omega\mathbf{E}$. By using $k = \omega/c$ relation, then potential vector $\mathbf{A}$ in vacuum becomes

$$\mathbf{A}_\rho = \frac{-i\mathbf{E}_\rho}{\omega}. \tag{4.8}$$

Where the energy density of the electromagnetic wave is denoted by I_ρ, the length of the Poynting vector is given by

$$I_\rho = \frac{E_\rho B_\rho}{\mu_0} = \frac{E_\rho^2}{\mu_0 c}. \tag{4.9}$$

Here the unit of I_ρ is [Joule/(m^{2}sec)]. The vector potential can be written in terms of light intensity I_ρ, and polarization of the electric field component $\mathbf{P}$ as

$$\mathbf{A}_\rho(t) = \frac{-i}{\omega}\sqrt{\frac{I_\rho}{c\epsilon_0}}\exp(\pm i\omega t)P. \tag{4.10}$$

The "±" sign corresponds to emission("+") or absorption ("−") of a photon with frequency ω. Here ϵ_0 is the dielectric constant of vacuum with units [F/m]. The matrix element for optical transitions from an initial state $\imath$ at $\mathbf{k} = \mathbf{k}_\imath$ to a final state f at $\mathbf{k} = \mathbf{k}_f$ is defined by

$$\mathbf{M}^{f\imath}_{\mathrm{opt}\rho}(\mathbf{k}_f, \mathbf{k}_\imath) = \big\langle \Psi^f(\mathbf{k}_f)|H_{\mathrm{opt}\rho}|\Psi^\imath(\mathbf{k}_\imath)\big\rangle. \tag{4.11}$$

The matrix element in Eq. (4.11) is calculated by

$$\mathbf{M}^{f\imath}_{\mathrm{opt}\rho}(\mathbf{k}_f, \mathbf{k}_\imath) = \frac{e\hbar}{m\omega_\rho}\sqrt{\frac{I_\rho}{\epsilon_0 c}}e^{i(\omega_f-\omega_\imath\pm\omega_\rho)t}\mathbf{D}^{f\imath}(\mathbf{k}_f, \mathbf{k}_\imath)\cdot\mathbf{P} \tag{4.12}$$

where

$$\mathbf{D}^{f\imath}(\mathbf{k}_f, \mathbf{k}_\imath) \quad = \quad \big\langle \Psi^f(\mathbf{k}_f)|\nabla|\Psi^\imath(\mathbf{k}_\imath)\big\rangle \tag{4.13}$$

is the dipole vector between initial states $\imath$ and final states f. Fermi's golden rule gives transition probability between the initial state $\imath$ and the final state f for interaction time τ with the perturbation. For Ψ^f and $\Psi^\imath$, we put the tight binding wavefunctions of the π electrons in graphene. Using Eqs. (4.5) and (4.10), we can write the optical absorption (A) and emission (E) probability per one second as as a function of $\mathbf{k}$.

$$\begin{aligned} W^{\rho=A,E}(\mathbf{k}_f,\mathbf{k}_\imath) &= \frac{4e^2\hbar^4 I_\rho}{\tau\epsilon_0 m^2 c^3 E_{\text{laser}}^2}|\mathbf{P}\cdot\mathbf{D}^{f\imath}(\mathbf{k}_f,\mathbf{k}_\imath)|^2 \\ &\times \frac{\sin^2[(E^f(\mathbf{k}_f)-E^\imath(\mathbf{k}_\imath)\pm E_{\text{laser}})\frac{\tau}{2\hbar}]}{(E^f(\mathbf{k}_f)-E^\imath(\mathbf{k}_\imath)\pm E_{\text{laser}})^2} \end{aligned} \tag{4.14}$$

Here, for absorption, $\rho = A$ goes with the “$-$” sign and emission $\rho = E$ goes with the “$+$” sign of “$\pm$”. To derive Eq. (4.14), we considered the light propagation in vacuum. The initial and final states can be valence or conduction bands $\imath, f = v$ or c. The meaning of I_ρ in Eq. (4.14) in the case of absorption of light and in the case of stimulated light emission is the intensity of the incoming light. The energy conservation $E^f(\mathbf{k}_f) - E^\imath(\mathbf{k}_\imath) \pm E_{\text{laser}} = 0$ is fulfilled for long interaction times τ because $\frac{\sin^2(\alpha t)}{\pi\alpha^2 t} \to \delta(\alpha)$ for $\tau \to \infty$.

In summary, in this section we have shown that the optical absorption intensity is proportional to the absolute square of the inner product of light polarization with dipole vector.

$$W(\mathbf{k}_f,\mathbf{k}_\imath) \propto \left|\mathbf{P}\cdot\mathbf{D}^{f\imath}(\mathbf{k}_f,\mathbf{k}_\imath)\right|^2 \tag{4.15}$$

In the following we derive an expression for the dipole vector for transitions connecting π and π^* bands.

4.2.2 Dipole vector

The wave function can be expressed as the sum of bloch functions for $2p_z$ orbitals of carbon atoms at A and B sublattice, Φ_A and Φ_b. Here we decompose Φ_A and Φ_b into atomic orbitals with bloch phase vector. There is a selection rules for the optical transition, the transition within a $2p_z$ orbital at the same atom is prohibited as a consequence of the odd symmetry of D in z. The z component of $\mathbf{D}^{fi}$ is zero for all atomic matrix element, and the transition between nearest neighbor atoms, which are also because of the odd symmetry of z component of $\mathbf{D}^{fi}$. The dipole vector can be written as

$$\begin{aligned} \mathbf{D}^{f\imath}(\mathbf{k}_f, \mathbf{k}_\imath) &= c_B^{f*}(\mathbf{k}_f) c_A^{\imath}(\mathbf{k}_\imath) \left\langle \Phi_B(\mathbf{k}_f, \mathbf{r}) | \nabla | \Phi_A(\mathbf{k}_\imath, \mathbf{r}) \right\rangle \\ &+ c_A^{f*}(\mathbf{k}_f) c_B^{\imath}(\mathbf{k}_\imath) \left\langle \Phi_A(\mathbf{k}_f, \mathbf{r}) | \nabla | \Phi_B(\mathbf{k}_\imath, \mathbf{r}) \right\rangle . \end{aligned} \tag{4.16}$$

The magnitude of the $\mathbf{D}^{fi} \cdot \mathbf{P}^{fi}$ describes the polarization dependence of W, which is calculated on the electron-equi energy contour for $E^f - E^i \pm E_{\text{laser}} = 0$. The+ sign is for emission and $-$ is for absorption of a photon. We substitute the Φ_A and Φ_b Bloch function, the Eq. (3.7) to the tight binding atomic wave function. The coordinates of all atoms in crystal can be split into $\mathbf{R}_A^j$ and $\mathbf{R}_B^j$ over the A and B sublattice, respectively. The vector which connect nearest neighbour starting from A(B) atom is defined in Eq. (3.19). $\mathbf{R}_A^j$ and $\mathbf{R}_B^j$ can be written as

$$\mathbf{R}_A^j = \mathbf{R}_B^i + \mathbf{r}_B^\ell, \quad \mathbf{R}_B^j = \mathbf{R}_A^i + \mathbf{r}_A^\ell, \quad (\ell = 1, 2, 3). \tag{4.17}$$

By substituting Eq. (3.7) into Eq. (4.16), we can get

$$\begin{aligned} \mathbf{D}^{cv}(\mathbf{k}_f, \mathbf{k}_\imath) &= \frac{1}{U} \sum_{i=0}^{U-1} \sum_{\ell=1}^{3} c_B^{c*}(\mathbf{k}_f) c_A^{v}(\mathbf{k}_\imath) \exp\left[i(\mathbf{k}_\imath - \mathbf{k}_f) \cdot \mathbf{R}_A^i\right] \\ & \quad \exp(-i\mathbf{k}_f \cdot \mathbf{r}_A^\ell) \left\langle \phi(\mathbf{r} - \mathbf{r}_A^\ell) | \nabla | \phi(\mathbf{r}) \right\rangle \\ &+ \frac{1}{U} \sum_{i=0}^{U-1} \sum_{\ell=1}^{3} c_A^{c*}(\mathbf{k}_f) c_B^{v}(\mathbf{k}_\imath) \exp\left[i(\mathbf{k}_\imath - \mathbf{k}_f) \cdot \mathbf{R}_B^i\right] \\ & \quad \exp(-i\mathbf{k}_f \cdot \mathbf{r}_B^\ell) \left\langle \phi(\mathbf{r} - \mathbf{r}_B^\ell) | \nabla | \phi(\mathbf{r}) \right\rangle , \end{aligned} \tag{4.18}$$

where c and v denote the conduction and valence band, repsctively. The summation over the atom $\mathbf{R}_A^i$ and $\mathbf{R}_B^i$ in Eq.(4.18) gives the selection rules for $\mathbf{k}$, only $\mathbf{k}_i = \mathbf{k}_f$ has a value, so the only vertical transition is possible. In the case of graphene the dipole vector is given by

$$\mathbf{D}^{f\imath}(\mathbf{k}) = \left\langle \Psi^f(\mathbf{k}) | \nabla | \Psi^\imath(\mathbf{k}) \right\rangle \cdot \tag{4.19}$$

The atomic dipole vector for A and B sublattice, $\mathbf{v}_{gA}$ and $\mathbf{v}_{gB}$ respectively, are given by

$$\begin{aligned}
\mathbf{v}_{gA}(\mathbf{k}) &= -\sum_{\ell}^{3} \exp(-i\mathbf{r}_A^{\ell}\cdot\mathbf{k}) \int \phi^*(\mathbf{r}-\mathbf{r}_A^{\ell})\nabla\phi(\mathbf{r})d\mathbf{r} \\
&= -\frac{\sqrt{3}m_{\text{opt}}}{a}\sum_{\ell}^{3}\exp(-i\mathbf{r}_A^{\ell}\cdot\mathbf{k})\mathbf{r}_A^{\ell} \\
\mathbf{v}_{gB}(\mathbf{k}) &= -\sum_{\ell}^{3} \exp(-i\mathbf{r}_B^{\ell}\cdot\mathbf{k}) \int \phi^*(\mathbf{r}-\mathbf{r}_B^{\ell})\nabla\phi(\mathbf{r})d\mathbf{r} \\
&= -\frac{\sqrt{3}m_{\text{opt}}}{a}\sum_{\ell}^{3}\exp(-i\mathbf{r}_B^{\ell}\cdot\mathbf{k})\mathbf{r}_B^{\ell} \qquad (4.20)
\end{aligned}$$

where $a/\sqrt{3}$ is the length of the $\mathbf{r}_B^{\ell}$ and $\mathbf{r}_A^{\ell}$ as defined in Eq. (3.19). m_{opt} is an atomic matrix element for nearest neighbor carbon pairs. m_{opt} describes the optical properties of π electrons in graphene and is given by

$$m_{\text{opt}} = \left\langle \phi(\mathbf{r}-\mathbf{r}_B^1) \left| \frac{\partial}{\partial x} \right| \phi(\mathbf{r}) \right\rangle . \qquad (4.21)$$

Since the product of the atomic wavefunction and its derivative quickly decreases with increasing the distance between the atoms, we consider only nearest neighbor coupling.

Since $c_A^{c*}c_B^v = -(c_B^{c*}c_A^v)^*$, which can be shown analytically by substituting the expressions for the wavefunction coefficients from Eq. (3.26), and $\mathbf{v}_{gA}^*(\mathbf{k}) = -\mathbf{v}_{gB}(\mathbf{k})$. From 4.20 we can write the dipole vector from Eq. (4.18) as $\mathbf{D}^{cv}(\mathbf{k}) = c_B^{c*}c_A^v\mathbf{v}_{gA} + c_A^{c*}c_B^v\mathbf{v}_{gB}$. Finally we get,

$$\mathbf{D}^{cv}(\mathbf{k}) = -\frac{2\sqrt{3}m_{\text{opt}}}{a}\text{Re}\left[c_B^{c*}(\mathbf{k})c_A^v(\mathbf{k})\sum_{l}\exp(-i\mathbf{r}_A^l\cdot\mathbf{k})\mathbf{r}_A^l\right] . \qquad (4.22)$$

According to the Eq.(4.22), $\mathbf{D}^{cv}$ is a real value of vector and its direction is depends on $\mathbf{k}$. The oscillator strength $O(\mathbf{k})$ in the unit of m_{opt} is given by

$$O(\mathbf{k}) = \sqrt{\mathbf{D}^{cv*}(\mathbf{k})\cdot\mathbf{D}^{cv}(\mathbf{k})}. \qquad (4.23)$$

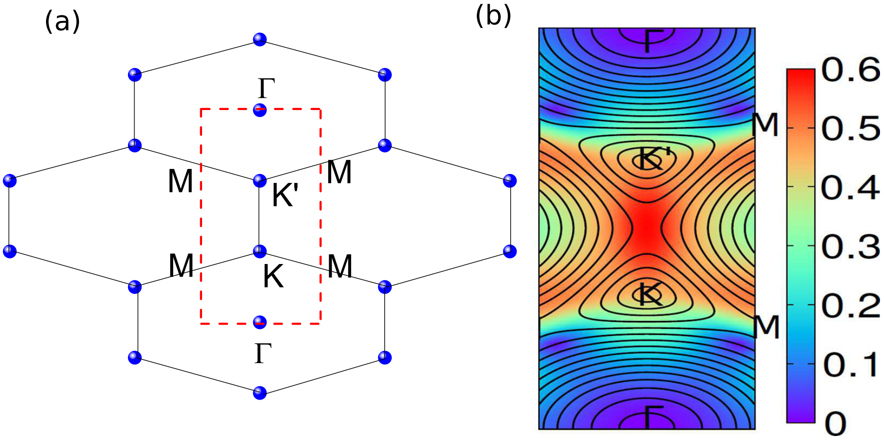

Figure 4.4 (a) Brillouin zone of graphene (b) The oscillator strength in units of m_{opt} as a funtion of $\mathbf{k}$ is plotted in the graphene Brillouin zone. The maximum value of oscillator strength is in the M point.

In Fig.4.4, we show the oscillator strength plotted in the Brillouin zone. The maximum value of $O(\mathbf{k})$ lies at the M point and minimum value of $O(\mathbf{k})$ lies at the Γ point.

4.3 Electron-phonon interactions

The displacement of the atom around the equilibrium position contributes to electron-phonon interaction. The displacement of the atom can be treated in first-order time-dependent perturbation theory. In the Raman intensity calculation, the electron-phonon information is very important, because the electron phonon interaction contributes to the numerator, as can be seen in Eqs.(4.2) and (4.1). The lifetime of photo-excited carrier also can be calculated from the electron-phonon interaction [6]. The matrix element of the electron-phonon interaction is determined by a scalar product of the derivative of the periodic potential V with respect to an atomic displacement vector in the ν-th phonon eigen vector [39, 52, 53, 54]. The electron-phonon

---

Fig. 4.4: picuse/dipolevector1.eps.eps

interaction matrix element from an initial state $\mathbf{k_i}$ to the final $\mathbf{k_f}$ electronic states can be written by

$$M^{b'\nu b}_{\text{el}-\text{ph}}(\mathbf{k}_f,\mathbf{q},\mathbf{k}_i)=\langle\Psi^{b'}(\mathbf{k}_f,\mathbf{r},t)|\delta V^{\nu}(\mathbf{q},\mathbf{r},t)|\Psi^{b}(\mathbf{k}_i,\mathbf{r},t)\rangle, \tag{4.24}$$

where $\Psi^b(\mathbf{k}_f,\mathbf{r},t)$ is the one-electron wave function in the b-th electronic energy band of Eq. (3.6), δV^ν is the variation of the periodic potential for the ν-th phonon mode, which is expressed by the deformation potential ∇v:

$$\delta V^{\nu}(\mathbf{q},\mathbf{r},t)=-\sum_{u's'}\nabla v(\mathbf{r}-\mathbf{R}_{u's'})\cdot S^{\nu}(\mathbf{R}_{u's'}), \tag{4.25}$$

where $v(\mathbf{r}-\mathbf{R}_{u's'})$ is the Kohn-Sham potential of a neutral pseudoatom moving along $\mathbf{R}_{u's'}$, and $S^\nu(\mathbf{R}_{u's'})$ is the site position deviation from the equilibrium site $\mathbf{R}_{u's'}$ caused by a vibration:

$$S^{\nu}(\mathbf{R}_{us})=\sqrt{\frac{\hbar n^{\nu}_{\pm}(\mathbf{q})}{2UM\omega^{\nu}(\mathbf{q})}}\mathbf{e}^{\nu}_{s}(\mathbf{q})e^{\mp i\left(\mathbf{q}\cdot\mathbf{R}_{us}-\omega^{\nu}(\mathbf{q})t\right)}, \tag{4.26}$$

where M is the carbon atom mass, U is the number of two atom unit cells, $\omega^\nu(\mathbf{q})$ is the $\nu-$th phonon frequency, $n^\nu_\pm(\mathbf{q})$ is the occupation number for the phonon absorption $(-)$ or phonon emission $(+)$. The phonon occupation number in the equilibrium position $n^\nu(\mathbf{q})$ is determined by the Bose-Einstein distribution function,

$$n^{\nu}(\mathbf{q})=\frac{1}{\exp\left[\,\hbar\omega^{\nu}(\mathbf{q})/k_BT\,\right]-1}, \tag{4.27}$$

where T and k_B, respectively, denote temperature and the Boltzman constant. By substituting Bloch wave function Eq. (3.6), deformation potential Eq. (4.25), and site position Eq.(4.26) into electron-phonon interaction matrix element Eq. (4.24), we can obtain the electron-phonon matrix element from $\mathbf{k_i}$ in the $b-$th energy band to $\mathbf{k_f}$ in the $b'-$th energy band coupled by the $\nu-$th phonon

$$M^{b'\nu b}_{\text{el}-\text{ph}}(\mathbf{k}_f,\mathbf{q},\mathbf{k}_i)=-\sqrt{\frac{\hbar n^{\nu}_{\pm}(\mathbf{q})}{2UM\omega^{\nu}(\mathbf{q})}}m^{b'\nu b}_{\text{el}-\text{ph}}(\mathbf{k}_f,\mathbf{q},\mathbf{k}_i). \tag{4.28}$$

In Eq. (4.28), $m^{b'\nu b}_{\mathrm{el-ph}}(\mathbf{k}_f,\mathbf{q},\mathbf{k}_i)$ is defined as following form:

$$m^{b'\nu b}_{\mathrm{el-ph}}(\mathbf{k}_f,\mathbf{q},\mathbf{k}_i) = \sum_{s'o'}\sum_{so} C^{b'*}_{s'o'}(\mathbf{k}_f)C^{b}_{so}(\mathbf{k}_i)D^{\nu}_{s'o'so}(\mathbf{k}_f,\mathbf{q},\mathbf{k}_i), \tag{4.29}$$

where $D^{\nu}_{s'o'so}(\mathbf{k}_f,\mathbf{q},\mathbf{k}_i)$ is the atomic deformation potential matrix element, and defined as following form:

$$\begin{aligned} &D^{\nu}_{s'o'so}(\mathbf{k}_f,\mathbf{q},\mathbf{k}_i) = \\ &\quad \sum_{u''s''} \langle \Phi_{s'o'}(\mathbf{k}_f,\mathbf{r})|\nabla v(\mathbf{r}-\mathbf{R}_{u''s''})\cdot \mathbf{e}^{\nu}_{s''}(\mathbf{q})e^{\mp i\left(\mathbf{q}\cdot\mathbf{R}_{u''s''}-\omega^{\nu}(\mathbf{q})t\right)}|\Phi_{so}(\mathbf{k}_i,\mathbf{r})\rangle, \end{aligned} \tag{4.30}$$

where $\Phi_{so}(\mathbf{k},\mathbf{r})$ is the Bloch wave function in Eq. (3.7). By keeping only two-center atomic matrix elements, $\mathbf{R}_{u''s''} = \mathbf{R}_{us}$, $\mathbf{R}_{u''s''} = \mathbf{R}_{u's'}$, and $\mathbf{R}_{u's'} = \mathbf{R}_{us}$, we can split Eq. (4.30) into three terms:

$$\begin{aligned} D^{\nu}_{s'o'so}(\mathbf{k}_f,\mathbf{q},\mathbf{k}_i) = \ & \sum_{u}^{U} \Big(\alpha_{o'o}(\mathbf{R}_{us}-\mathbf{R}_{u's'})\cdot\mathbf{e}^{\nu}_{s'}(\mathbf{q})\Big)e^{-i\mathbf{k}_f(\mathbf{R}_{us}-\mathbf{R}_{u's'})} \\ & + \Big(\beta_{o'o}(\mathbf{R}_{us}-\mathbf{R}_{u's'})\cdot\mathbf{e}^{\nu}_{s'}(\mathbf{q})\Big)e^{i\mathbf{k}_i(\mathbf{R}_{us}-\mathbf{R}_{u's'})} \\ & + \Big(\lambda_{o'o}(\mathbf{R}_{us}-\mathbf{R}_{u's'})\cdot\mathbf{e}^{\nu}_{s'}(\mathbf{q})\Big)e^{\pm i\mathbf{q}(\mathbf{R}_{us}-\mathbf{R}_{u's'})}, \end{aligned} \tag{4.31}$$

where the atomic deformation potential vector $\alpha_{o'o}(\mathbf{R})$, $\beta_{o'o}(\mathbf{R})$, and $\lambda_{o'o}(\mathbf{R})$ are defined as follows [53, 55]:

$$\begin{cases} \alpha_{o'o}(\mathbf{R}) = \displaystyle\int \phi^{*}_{o'}(\mathbf{r})\nabla v(\mathbf{r}-\mathbf{R})\phi_{o}(\mathbf{r}-\mathbf{R})d\mathbf{r}, \\ \beta_{o'o}(\mathbf{R}) = \displaystyle\int \phi^{*}_{o'}(\mathbf{r})\nabla v(\mathbf{r})\phi_{o}(\mathbf{r}-\mathbf{R})d\mathbf{r}, \\ \lambda_{o'o}(\mathbf{R}) = \displaystyle\int \phi^{*}_{o'}(\mathbf{r})\nabla v(\mathbf{r}-\mathbf{R})\phi_{o}(\mathbf{r})d\mathbf{r}, \end{cases} \tag{4.32}$$

where $\phi_o(\mathbf{r})$, $\alpha_{o'o}(\mathbf{R})$ and $\beta_{o'o}(\mathbf{R})$, respectively are the atomic wave function for the o-th orbital, the off-site atomic deformation potential vectors, and the on-site atomic deformation potential vector. $\mathbf{R}$ connects the two interacting atoms.

Chapter 5

G* band Raman spectra of graphene

In this chapter we show the calculated G* band spectra. We also assign the G* band and we conclude the origin of G* band.

5.1 Origin of G* band

The G* band spectra of monolayer graphene is a double resonance Raman spectrum. We calculate the possible process for G* band based on the previous work done by T. Shimada [14], D.L. Mafra [15] and R. Saito [8]. There are four possibilities to obtain the G* band ; (1) $q = 0$, overtone of LO phonon,(2) $q = 2k$, iTO and LA combination phonon mode, (3) $q = 0$, LO and iTA combination phonons, (4) $q = 0$, overtone of iTO. Phonon wavevector is measured from K point as explained in Chapter 4.

Based on experimental result G* band peak position shifts to lower Raman shift with increasing laser energy. As a consequence the calculated Raman spectra of G* band should follow those behavior. The calculated Raman spectra based on four possibilities can be seen in Fig. 5.1. In Fig. 5.1(a), we show the calculated Raman spectra with phonon wave vector $q = 0$, overtone of LO. The peak positions for 785 nm and 532 nm are 2480

Fig. 5.1: picuse/ramangstar.eps

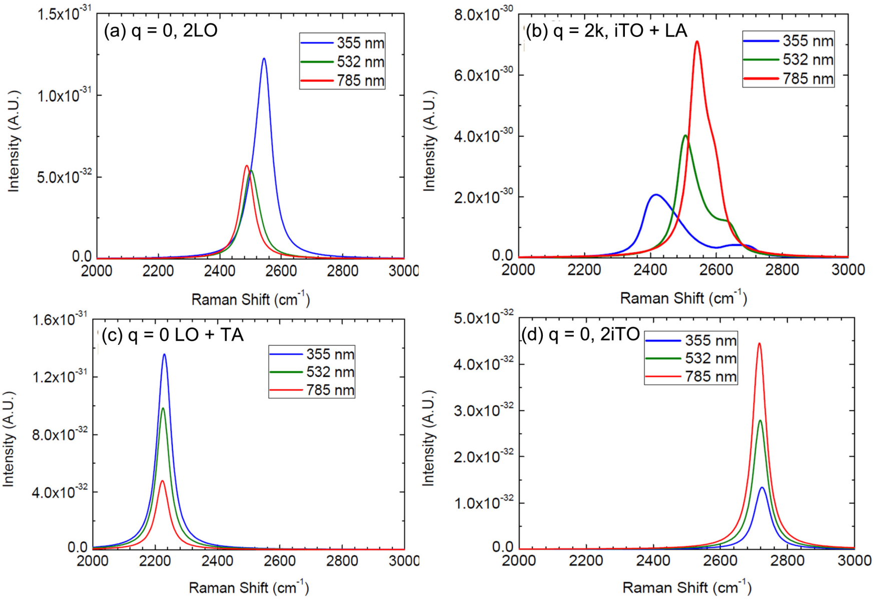

Figure 5.1 Theoretical result for G* band spectra for several laser excitation energy; 355 nm, 532 nm, and 785 nm. (a)$q = 0$, overtone of LO phonon, (b)$q = 2k$, iTO and LA combination phonon mode,(c)$q = 0$, LO and TA combination phonon mode, and (d) $q = 0$, overtone of iTO phonon. The $q = 2k$ gives highest intensity and the peak position shifts with increasing E_L.

cm^{-1} and for 355 nm the peak position is 2520 cm^{-1}.

In Fig. 5.1(b), we show the Raman spectra with phonon wave vector $q = 2k$, iTO and LA combination phonon modes. The peak position shifts to lower Raman shift with increasing E_L.

In Fig. 5.1(c), we show the Raman spectra with phonon wave vector $q = 0$, LO and TA combination phonon modes. The peak positions are around 2200 cm^{-1} and are constant in respect to E_L. In Fig. 5.1(d), we show the Raman spectra with phonon wave vector $q = 0$, overtone of iTO. The peak position are around 2700 cm^{-1} and constant to E_L. The summary of four possibilities of calculated G* spectra can be seen in Tab. 5.1.

Based on calculation result in Fig. 5.1, we can conclude that the $q = 0$ gives the peak positions constant to E_L. However for $q = 0$ overtone of LO,

Table 5.1: The peak intensities value of the calculated result from Fig. 5.1. Bold numbers denote the highest intensity.

E_L	(q=0) 2LO	(q=2k) iTO+LA	(q=0) 2iTO	(q=0) LO+TA
355 nm	1.2×10^{-31}	$\mathbf{2.0 \times 10^{-30}}$	1.0×10^{-32}	1.4×10^{-31}
532 nm	5.0×10^{-32}	$\mathbf{4.2 \times 10^{-30}}$	3.0×10^{-32}	1.0×10^{-31}
785 nm	5.1×10^{-32}	$\mathbf{7.0 \times 10^{-30}}$	4.5×10^{-32}	4.2×10^{-31}

the peak position is shifted as shown in Fig. 5.1(a), this distortion is caused by the numerical error.

Based on Raman intensity calculation from the four possibilities to assign the G* band, we can see that iTO and LA combination phonon mode gives highest intensity compare to another combination phonon modes, beside that the iTO and LA combination phonon modes show the peak intensity shifts as a function of E_L. Hence, we can conclude that the phonon contributing to the G* band are iTO and LA combination mode with phonon wavevector $q = 2k$ measured from K point.

5.2 Calculation result of G* band

In this Section, we show the calculation result of G* band. The assignment for G* band that we use in this section are iTO and LA combination phonon modes, with phonon wave vector, $q = 2k$.

In Fig. 5.2, we show the calculated peak position of G* band as a function of E_L. The calculated peak position are slightly higher than experimental results. This discrepancy is caused by the phonon energy dispersion calculated by using force constant model that we used to calculate Raman intensity can not reproduce experimental result as explained in Sec. 3.3. In order to get better result, we calculate the phonon energy dispersion by using quantum espresso package, the calculation result can be seen in Fig. 5.3.

Fig. 5.2: picuse/gstarexpcalpeak.eps
Fig. 5.3: picuse/phonondis.eps

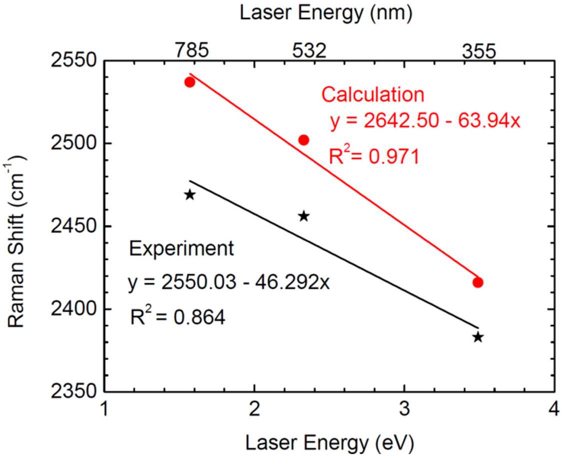

Figure 5.2 The G* band peak position as a function of E_L fitted with linear function, black(experiment) and red(calculation).

In Fig. 5.3, we show the calculated phonon energy dispersion using Quantum Espresso. Calculated phonon energy dispersion using Quantum Espresso gives better result than calculated phonon energy dispersion using force constant model near the K point.

We recalculate the Raman intensity of G* band with phonon frequency obtained from Quantum Espresso package. Therefore we do not calculate the electron-phonon matrix element from Quantum Espresso. Thus, we use the calculated electron-phonon matrix element from tight-binding calculation, the same with previous calculation.

In Fig. 5.4(a), we show the calculation result of Raman spectra of G* band fitted with experimental result [7]. The intensities are normalized with its G* band peaks. The calculated result is in good agreement with experimental result, however for 355 nm laser, the calculation result is broader than experimental result. The G* band peak position as function of E_L can be seen in Fig. 5.4(b). The calculated Raman intensity with phonon energy dispersion obtained from Quantum Espresso can reproduce the experimental

---

Fig. 5.4: picuse/qegstarexp.eps

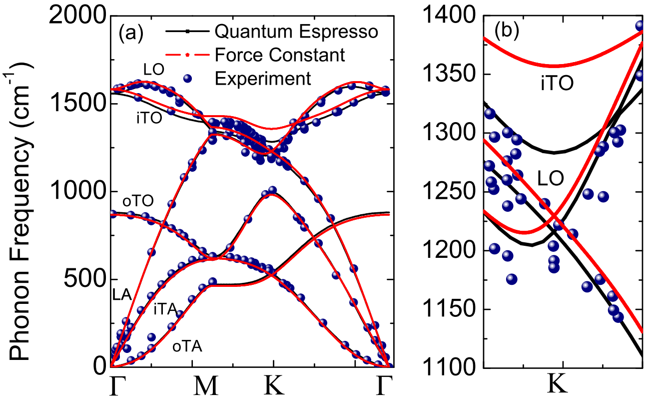

Figure 5.3 (a) Phonon energy dispersion relation of graphene calculated using force constant model (red lines), and quantum expresso (black lines), fitted with experiment data of the X-ray inelastic scattering in graphene (blue dots) by A. Grüneis *et al* [35], plotted along high symmetry direction. (b) The phonon energy dispersion near the K point for iTO and LO phonon modes. Phonon energy dispersion calculated by using quantum espresso reproduce the experimental result near K point.

result of peak position. The peak positions are exactly the same with the experimental result. The peak position shifts with increasing E_L, with slope -41.30 cm^{-1}/eV. Previous work reported the dispersive behavior of G* is -10 to -20 cm^{-1}/eV [26, 23]. However, in our calculation and experimental data, we just have three different E_L, and the peak intensity of G* band is low, as a consequence it is difficult to distinguish peak and background.

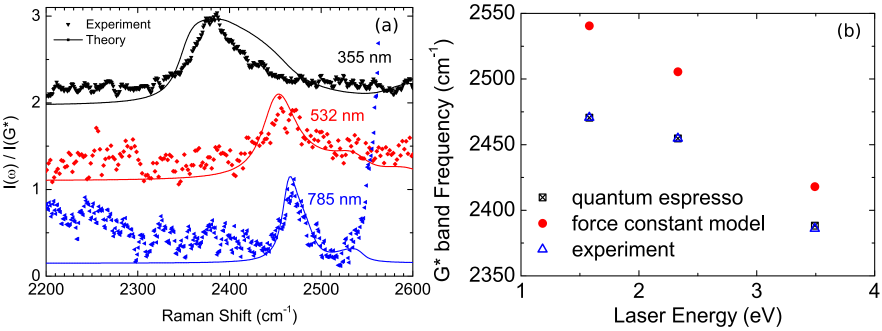

Figure 5.4 Calculation result of (a) Raman intensity of G* band with phonon frequency calculated by using Quantum Espresso Package and (b) G* band peak position as a function of laser energy fitted with experimental result [7].

Chapter 6

G′ band Raman spectra of Graphene

In this chapter, we show the origin of G′ band, and also E_L dependence of the peak position and peak intensity.

6.1 Origin of G′ band

Based on the experimental result shown in Fig. 2.1, the peak position of G′ band is shifted as a function of the E_L. Thus, the G′ band process is double resonance process with phonon wave vector $q = 2k$ measured from the K point. We explain the origin of the G′ band based on the calculated result.

We calculate the Raman intensity using Eq. (4.2). According to the experimental result, the G′ band peak position is around 2700 cm^{-1}. Therefore the G′ band should be overtone or combination phonon, because according to the phonon energy dispersion, the maximum of frequency is around 1600 cm^{-1}. We assign the phonon contributing to the G′ band based on the phonon energy dispersion as shown in Fig. 3.6. In order to assign G′ band, we devide the frequency by two, 1350 cm^{-1}. The corresponding phonon with 1350 cm^{-1} near K point are LO, iTO, or LA. According to the calculation

---

Fig. 6.1: picuse/gpas.eps

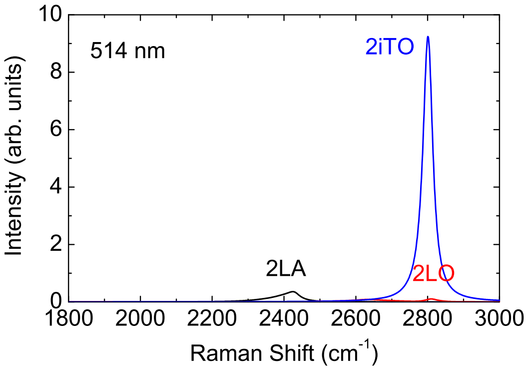

Figure 6.1 Calculation result of Raman spectra of monolayer graphene to assign G′ band based on double resonance Raman. Black line, blue line and red line, respectively denote overtone of LA, overtone of iTO and overtone of LO. Overtone of iTO gives highest intensity

result as shown in Fig. 6.1, we can conclude the phonon contributing to the G′ band is overtone of iTO. We use the overtone of iTO to calculate the G′ band in this master thesis.

6.2 Calculated result of G′ band

We calculate the Raman intensity of G′ band using Eq. (4.2). The calculation result can be seen in Fig. 6.2. The Peak intensity of G′ band is decreasing by increasing laser excitation energy, these result are similar with the experimental result as shown in Fig. 2.1(a).

6.3 Disspersive behavior of G′ band

Our calculated G′ band spectra also show the disspersive behaviour of G′ band.

Fig. 6.2: picuse/gpband.eps
Fig. 6.3: picuse/gprimepeak.eps

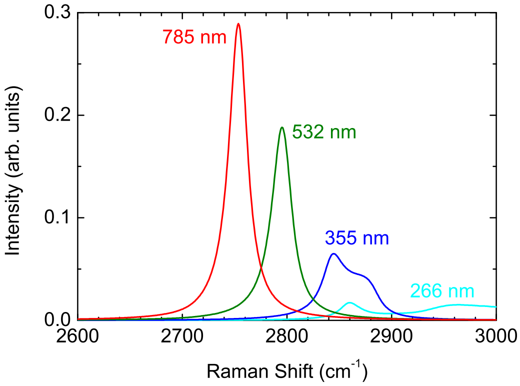

Figure 6.2 The calculation result of Raman spectra of G′ band excited by several laser excitation energy : 266 nm, 355 nm, 532 nm and 785 nm. The peak intensity decreases with increasing E_L.

In Fig. 6.3 we plot calculated frequency of G′ band as a function of E_L. The peak position of G′ band shifts linearly to higher frequencies with increasing the E_L as shown in Fig. 6.3. The observed phonon energy increases by increasing the E_L, which gives rise to a dispersive behavior of the scattered phonon [6]. Since the electronic energy dispersion of the π and $\pi^\star$ bands is linear in k as measured from the K (K') point in the 2D Brillouin zone of graphene, a special k value is selected on an equi-energy line for a given laser energy [26].

The calculated slope of phonon frequency in Fig.6.3 is 48 cm^{-1}/eV. Our results are lower compared to the previous experimental result [23, 24, 25]. From previous experimental reported in the literature for graphene, the slope is 85-107 cm^{-1}/eV [23, 24, 25]. This discrepancy might be caused by the iTO phonon energy dispersion based on force constant model that we used, near K point are not reproduced experimental result as explained in Section 3.3. However, this result is still good, because we can reproduce the linear relation of peak position and E_L and also we can reproduce the peak intensity decreases with increasing E_L.

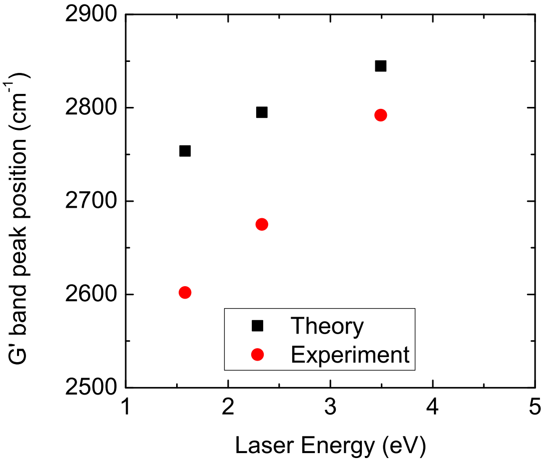

Figure 6.3 G′ band peak position as a function of laser excitation energy fitted with experiment data [7].

6.4 Spectral width of G′ band

We fitted the calculated result of Raman spectra in Fig. 6.2 with Lorentzian function. The Lorentzian fitting function is given by

$$I(\omega) = \frac{I_0}{\pi \Gamma_q} \frac{1}{(\omega - \omega_q)^2 + \Gamma_q^2} \tag{6.1}$$

In 6.1 full width at half maximum (FWHM) or spectral line width is given by FWHM $= 2\Gamma_q$. The spectral line width has important information, such as damping, the energy uncertainty, and the phonon lifetime. Therefore, Γ_q is the inverse of the lifetime for a phonon. The origins for the finite phonon lifetime is the electron-phonon interaction [26].

Calculation result shows the spectral line width of the G′ band increases slightly from the near infrared 785 nm (26 cm^{-1}) to the visible 532 nm (27 cm^{-1}) light. However, this value increases by a factor of 1.5 when an ultraviolet laser (355 nm) is used.

The E_L dependence of the calculated spectral line width of the G′ band

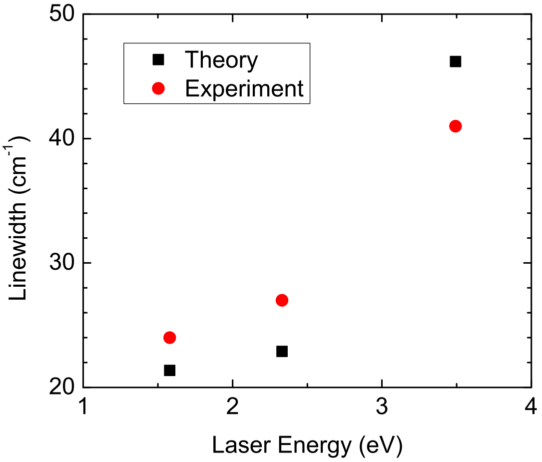

Figure 6.4 Spectral line width of G′ band fitted with experiment data [7].

is in a good agreement with the trend of curve with the experimental data as shown in Fig.6.4. However, the experimental results are slightly higher than calculations results. The discrepancies might be caused by the value of resonance window that we set constant, $\gamma_r = 0.1$ eV in Eq. (4.2) is not sufficient. The resonance window is a function of E_L. However, the calculation result shows the calculated line width of the spectra is still in good agreement with experimental result.

6.5 Integrated intensity of G′ band

In this section we calculate the integrated intensity of Raman spectra to analyze the absence of G′ band in 266 nm E_L. The area under the curve is defined as integrated intensity. Integrated intensity is important because its free from the sample size, as a consequence we can compare with experimental result.

Fig. 6.4: picuse/linewidth.eps

We plot the calculated results of the absolute Raman spectra of monolayer graphene in Fig. 6.5(a). We see that the integrated intensity of the G (G′) band is proportional to E_L^4 (E_L^{-1}), as shown in Fig. 6.5(b) [Fig. 6.5(c)]. Therefore, the integrated intensity ratio of the G′ to band is inversely proportional to the fifth power of the incident laser energy. A similar E_L dependence of the integrated intensity of certain Raman phonon modes has been reported in nanographite [56] and graphene [43].

The calculated results of the integrated intensity of the G′ band proportional to E_L^{-1} with the constant resonance Raman window γ_r reproduce the experimental data for large E_L region.

6.6 Effect of deep ultraviolet laser to the G′ band peak

In this section, we discuss about the effect of the deep ultraviolet to the G G′ band peak. We only consider the optical transition between π band to $\pi^\star$ band.

When the E_L increases, the area of resonance condition shown by equi-energy contour in Fig. 6.6(a) increases. The increase of this area corresponds to the increased range of possible phonon momentum that can be excited near the K point in double resonance scattering. However, if we use E_L more than 5.08 eV, the equi-energy contour in K point is vanished, because 5.08 eV is M point transition as shown in Fig. 6.7(a).

In Fig. 6.6, we show the method to select the phonon wave vector q. If the E_L is less than 5.08 eV, the ordinary double resonance process occurs as shown in Fig. 6.6 (a) and for E_L higher than 5.08 eV, the the equi-energy contour calculated in Γ point and the possible phonon wave vector becomes a whole Brillouin zone as shown in Fig. 6.6(b).

Fig. 6.5: picuse/integrated.eps
Fig. 6.6: picuse/gabu.eps
Fig. 6.7: picuse/deepuv.eps

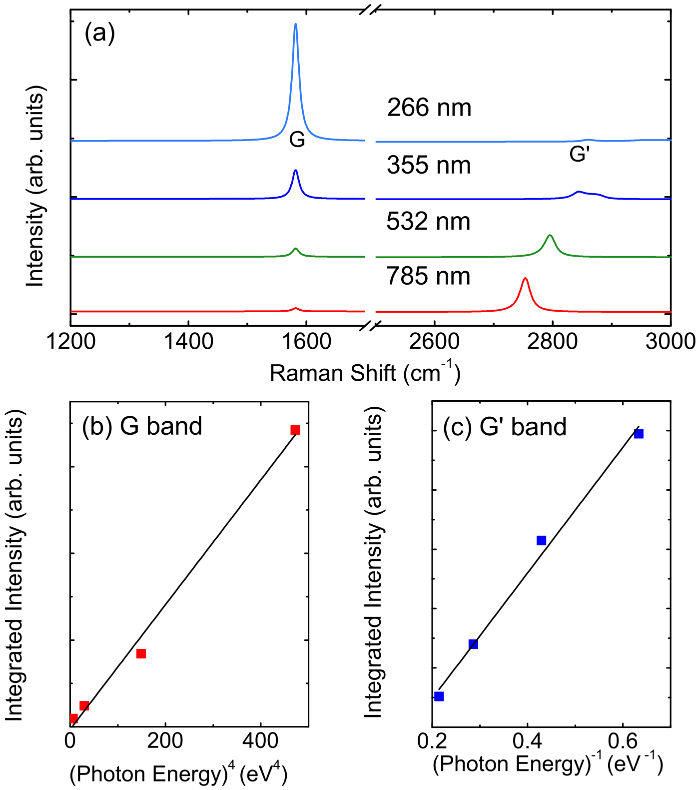

Figure 6.5 The calculated results of (a) the absolute Raman scattering spectra of monolayer graphene. (b) The integrated intensity of the G band as a function of E_L^4 fitted to a linear function. (c) The integrated intensity of the G′ band as a function of E_L^{-1} fitted to a linear function. [7].

In Fig.6.7(a), we show the electronic energy dispersion of graphene. The calculated Raman spectra by using E_L from 785 nm up to 190.8 nm can is shown in Fig.6.7(b). The peak intensity of G′ band is inversely proportional to the E_L as shown in inset of Fig.6.7(b).

In Fig. 6.8, we show the G′ band peak position as a function of E_L, the error bars represent the spectral width (FWHM). In the E_L more than 4.6 eV area, double peaks appear and the spectral width become large.

Although, we derive the double resonance process for deep ultraviolet

---

Fig. 6.8: picuse/peakdeep.eps

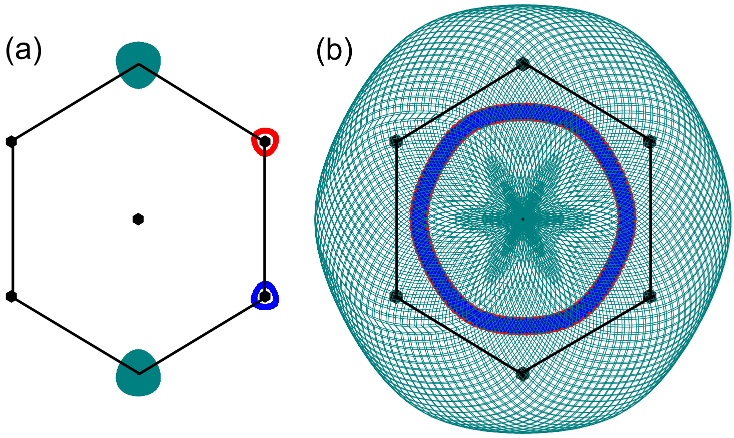

EL < 5.08 eV

EL > 5.08 eV

Figure 6.6 Equi-energy contours for incident laser energy (a) E_L less than 5.08 eV (b) E_L higher than 5.08 eV.

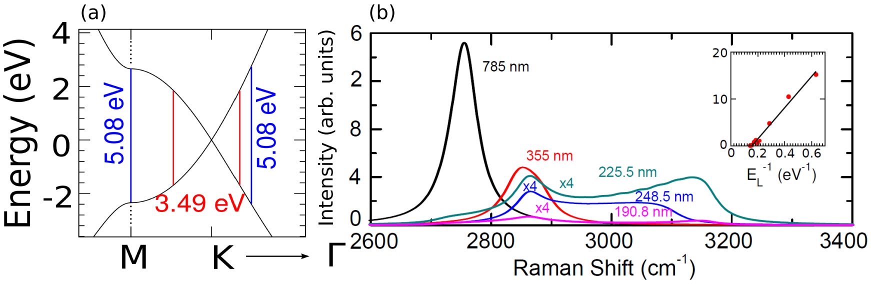

Figure 6.7 (a) Energy dispersion of monolayer graphene. The 5.08 eV laser energy correspond to the M point maximum. (b) The Raman spectra of monolayer graphene excited by 785 nm laser up to 190.8 nm.

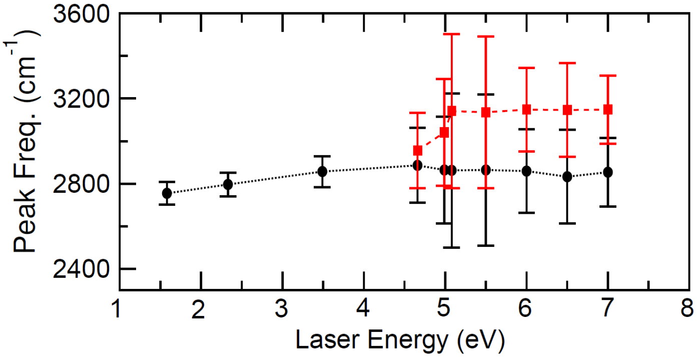

Figure 6.8 G′ band peak position as a function of E_L. when $E_L \geqslant 4.66$ eV, double peaks (red and black points) appear. Error bars represent the full width at half maximum (FWHM) of peak. When $E_L \geq 4.6$ eV , double peak (red and black) appear.

laser energy, the experimentalist can not observe the G′ band with deep ultraviolet laser, because the intensity is very weak, as a consequence the G′ band intensity is negligible compared with that of G band. Since the intensity ratio of G′ band to the G band is frequently used for characterizing the number of graphene layer [13, 27].

Chapter 7

Conclusion

In this thesis we calculated G* and G$'$ bands Raman spectra of monolayer graphene based on double resonance Raman theory. The double resonance Raman theory needs the electron-photon matrix elements, electron-phonon matrix elements and phonon energy dispersion. Here we list main results of the thesis.

Assignment of G* band process

Based on the explained calculation result in Chapter 5, we can conclude that the G* band process is double resonance Raman process. The phonon contributing the G* band are iTO and LA combination phonon mode with phonon wave vector $q = 2k$ measured from K point. The G* band peak position is sensitive to the E_L. The peak position shifts to the lower Raman shift with increasing the E_L. However the calculation result of G* band by using phonon energy dispersion from force constant model gives higher peak position than experimental result. We recalculate the Raman intensity of G* band by using the same formula, but the phonon energy dispersion obtained from quantum espresso. We successful reproduce the peak position of G* band experimental result, because the calculated phonon energy dispersion from Quantum Espresso almost reproduce the experimental result of phonon energy dispersion near K point.

Effect of increasing E_L to the G$'$ band spectra

The peak intensity of G$'$ band is inversely proportional to the E_L. In the case of $E_L \leq 5.08$ eV, the double resonance process with the equi-energy contour measured in K point occurs. The peak position is proportional to the E_L. The calculated slope is 48 cm^{-1}/eV.

In the case of $E_L > 5.08$ eV, the equi-energy contour will be measured around Γ point. The 5.08 eV becomes special value, because the 5.08 eV is the M point transition. In the case of laser energy more than 266 nm (4.66 eV) the G$'$ band intensity is very weak and negligible compared with that of G band. However, the absolute intensity of G* band still exists with very small intensity.

Appendix A

Calculation Programs

There are several programs used in this thesis. All the programs can be found under the following directory in FLEX workstation:

```
$ ~siregar/for/code/
```

For simplicity, this directory will defined as root. Please read 00Readme for each program.

Phonon energy dispersion

```
Directory : root/Phonondispersion/fcflat/
Main Program : tfcflat.for
```

Using tfcflat.for we can calculate the phonon energy dispersion, consider up to twentieth nearest neighbors in high symmetry points.

Electron-photon interaction

```
Directory : root/dipolevector/
Main Program : dipolevec.f90
```

Using dipoleve.f90 we can calculate dipolevector in whole Brillouin zone of monolayer graphene.

Electron-phonon interaction

`Directory : root/elphonon/`

`Main Program : nteplat.f90`

Using nteplat.f90 we can calculate the electron-phonon matrix element for each phonon branch.

First-order Raman scattering

The G band Raman spectra of graphene can be calculated by using gbandnew.f90

`Directory : root/ramanori/`

`Main Program : gbandnew.f90`

Second-order Raman scattering

Phonon energy dispersion from FCM

$G^\star$ band

`Directory : root/gstar150409/`

`Main Program : ramanqeori.f90`

G' band

`Directory : root/gpband/`

`Main Program : 785.f90`

G' band in deep ultraviolet

`Directory : root/deepuvraman/`

`Main Program : deepuv.f90`

Phonon energy dispersion from quantum espresso

$G^{\star}$ band

`Directory : root/gstar150409/`

`Main Program : gstarspectra.f90`

Publication list

Journal

1. Hsiang-Lin Liu, Syahril Siregar, Eddwi H Hasdeo, Yasuaki Kumamoto, Chih-Chiang Shen, Chia-Chin Cheng, Lain-Jong Li, Riichiro Saito, Satoshi Kawata., Deep-ultraviolet Raman scattering studies of monolayer graphene thin films, Carbon 81(0), 807-813(2015).

2. Riichiro Saito, Ahmad R.T. Nugraha, Eddwi H. Hasdeo, Syahril Siregar, Huaihong Guo, Teng Yang., phys. status solidi B, 1-12(2015).

Oral presentation

1. Syahril Siregar and Riichiro Saito : Absence of Raman G′ band in ultraviolet excitation regime of graphene, ATI 2014 Nano-Carbon Meeting, Yamagata-Zao, (2014.7.31-8.1).

Poster

1. Syahril Siregar, E.H. Hasdeo, A.R.T. Nugraha, R. Saito: Absence of Raman G′ band by ultraviolet excitation in monolayer graphene systems, Fullerene Nanotubes General Symposium, Nagoya University (2014.9.3-5).

2. Syahril Siregar, Eddwi H. Hasdeo, Ahmad R.T. Nugraha, Hsiang Liu, Riichiro Saito: $G^\star$ band Raman spectra of single layer graphene revisited, Fullerene Nanotubes General Symposium, The University of Tokyo (2015.2.21-23).

Bibliography

[1] P. R. Wallace, Phys. Rev. 71, 622–634 (May 1947).

[2] Chunxiao Cong, Ting Yu, Riichiro Saito, Gene F. Dresselhaus, and Mildred S. Dresselhaus, ACS Nano 5(3), 1600–1605 (2011). PMID: 21344883.

[3] L.M. Malard, M.A. Pimenta, G. Dresselhaus, and M.S. Dresselhaus, Physics Reports 473(56), 51 – 87 (2009).

[4] J. F. Rodriguez-Nieva, R. Saito, S. D. Costa, and M. S. Dresselhaus, Phys. Rev. B 85, 245406 (Jun 2012).

[5] Duhee Yoon, Young-Woo Son, and Hyeonsik Cheong, Phys. Rev. Lett. 106, 155502 (Apr 2011).

[6] Ado Jorio, Mildred S Dresselhaus, Riichiro Saito, and Gene Dresselhaus, Raman spectroscopy in graphene related systems (John Wiley & Sons, Singapore, 2011).

[7] Hsiang-Lin Liu, Syahril Siregar, Eddwi H. Hasdeo, Yasuaki Kumamoto, Chih-Chiang Shen, Chia-Chin Cheng, Lain-Jong Li, Riichiro Saito, and Satoshi Kawata, Carbon 81(0), 807 – 813 (2015).

[8] R. Saito, K. Sato, P.T. Araujo, D.L. Mafra, and M.S. Dresselhaus, Solid State Communications 175176(0), 18 – 34 (2013). Special Issue: Graphene V: Recent Advances in Studies of Graphene and Graphene analogues.

[9] Mildred S. Dresselhaus, Ado Jorio, Mario Hofmann, Gene Dresselhaus, and Riichiro Saito, Nano Letters 10(3), 751–758 (2010). PMID: 20085345.

[10] Johan Ek-Weis, Sara Costa, Otakar Frank, and Martin Kalbac, The Journal of Physical Chemistry Letters 5(3), 549–554 (2014).

[11] I. Calizo, A. A. Balandin, W. Bao, F. Miao, and C. N. Lau, Nano Letters 7(9), 2645–2649 (2007). PMID: 17718584.

[12] Ying ying Wang, Zhen hua Ni, Ting Yu, Ze Xiang Shen, Hao min Wang, Yi hong Wu, Wei Chen, and Andrew Thye Shen Wee, The Journal of Physical Chemistry C 112(29), 10637–10640 (2008).

[13] J.S. Park, A. Reina, R. Saito, J. Kong, G. Dresselhaus, and M.S. Dresselhaus, Carbon 47(5), 1303 – 1310 (2009).

[14] T. Shimada, T. Sugai, C. Fantini, M. Souza, L.G. Cançado, A. Jorio, M.A. Pimenta, R. Saito, A. Grüneis, G. Dresselhaus, M.S. Dresselhaus, Y. Ohno, T. Mizutani, and H. Shinohara, Carbon 43(5), 1049 – 1054 (2005).

[15] DL Mafra, G Samsonidze, LM Malard, DC Elias, JC Brant, F Plentz, ES Alves, and MA Pimenta, Physical Review B 76(23), 233407 (2007).

[16] Riichiro Saito and Hiromichi Kataura. Optical properties and Raman spectroscopy of carbon nanotubes. In Carbon nanotubes, pages 213–247, Springer, 2001.

[17] R Saito, A Grueneis, LG Cançcado, MA Pimenta, A Jorio, G Dresselhaus, MS Dresselhaus, et al. In MRS Proceedings, pages Z9–3. Cambridge Univ Press, 2001.

[18] AG Souza Filho, A Jorio, JH Hafner, CM Lieber, R Saito, MA Pimenta, G Dresselhaus, and MS Dresselhaus, Physical Review B 63(24), 241404 (2001).

[19] Mildred S Dresselhaus, G Dresselhaus, R Saito, and A Jorio, Physics reports 409(2), 47–99 (2005).

[20] MS Dresselhaus, G Dresselhaus, A Jorio, AG Souza Filho, and R Saito, Carbon 40(12), 2043–2061 (2002).

[21] J. Jiang, R. Saito, A. Grüneis, G. Dresselhaus, and M.S. Dresselhaus, Carbon 42(15), 3169 – 3176 (2004).

[22] A. Grüneis, R. Saito, Ge. G. Samsonidze, T. Kimura, M. A. Pimenta, A. Jorio, A. G. Souza Filho, G. Dresselhaus, and M. S. Dresselhaus, Phys. Rev. B 67, 165402 (Apr 2003).

[23] D. L. Mafra, G. Samsonidze, L. M. Malard, D. C. Elias, J. C. Brant, F. Plentz, E. S. Alves, and M. A. Pimenta, Phys. Rev. B 76, 233407 (Dec 2007).

[24] Irene Calizo, Igor Bejenari, Muhammad Rahman, Guanxiong Liu, and Alexander A. Balandin, Journal of Applied Physics 106(4), – (2009).

[25] C. Casiraghi, S. Pisana, K. S. Novoselov, A. K. Geim, and A. C. Ferrari, Applied Physics Letters 91(23), – (2007).

[26] R. Saito, M. Hofmann, G. Dresselhaus, A. Jorio, and M. S. Dresselhaus, Advances in Physics 60(3), 413–550 (2011).

[27] A. C. Ferrari, J. C. Meyer, V. Scardaci, C. Casiraghi, M. Lazzeri, F. Mauri, S. Piscanec, D. Jiang, K. S. Novoselov, S. Roth, and A. K. Geim, Phys. Rev. Lett. 97, 187401 (Oct 2006).

[28] Otakar Frank, Marcel Mohr, Janina Maultzsch, Christian Thomsen, Ibtsam Riaz, Rashid Jalil, Kostya S. Novoselov, Georgia Tsoukleri, John Parthenios, Konstantinos Papagelis, Ladislav Kavan, and Costas Galiotis, ACS Nano 5(3), 2231–2239 (2011). PMID: 21319849.

[29] Valentin N. Popov and Philippe Lambin, Carbon 54, 86 – 93 (2013).

[30] R. Saito, G. Dresselhaus, and M.S. Dresselhaus, Physical Properties of Carbon Nanotubes (Imperial College Press, London, 1998).

[31] J. C. Slater and G. F. Koster, Phys. Rev. 94, 1498–1524 (Jun 1954).

[32] A. Grüneis. Resonance Raman Spectroscopy of Single Wall Carbon Nanotubes. Ph. D. thesis, Tohoku University, Department of Physics, September 2004.

[33] O. Dubay and G. Kresse, Phys. Rev. B 67, 035401 (Jan 2003).

[34] O. Dubay, G. Kresse, and H. Kuzmany, Phys. Rev. Lett. 88, 235506 (May 2002).

[35] A. Grüneis, J. Serrano, A. Bosak, M. Lazzeri, S. L. Molodtsov, L. Wirtz, C. Attaccalite, M. Krisch, A. Rubio, F. Mauri, and T. Pichler, Phys. Rev. B 80, 085423 (Aug 2009).

[36] Janina Zimmermann, Pasquale Pavone, and Gianaurelio Cuniberti, Phys. Rev. B 78, 045410 (Jul 2008).

[37] J. Maultzsch, S. Reich, C. Thomsen, H. Requardt, and P. Ordejón, Phys. Rev. Lett. 92, 075501 (Feb 2004).

[38] L. Lindsay and D. A. Broido, Phys. Rev. B 81, 205441 (May 2010).

[39] J.S. Park. Double Resonance Raman Spectroscopy of Single Wall Carbon Nanotubes and Graphene. Ph. D. thesis, Tohoku University, Department of Physics, September 2008.

[40] R Saito, M Furukawa, G Dresselhaus, and MS Dresselhaus, Journal of Physics: Condensed Matter 22(33), 334203 (2010).

[41] RM Martin, LM Falicov, and M Cardona, Topics in applied Physics 8, 79 (1975).

[42] Manuel Cardona and Roberto Merlin, , 2007).

[43] Pedro Venezuela, Michele Lazzeri, and Francesco Mauri, Phys. Rev. B 84, 035433 (Jul 2011).

[44] D. M. Basko, Phys. Rev. B 76, 081405 (Aug 2007).

[45] Andrea C Ferrari and Denis M Basko, Nature nanotechnology 8(4), 235–246 (2013).

[46] MA Pimenta, G Dresselhaus, Mildred S Dresselhaus, LG Cancado, Ado Jorio, and R Saito, Physical chemistry chemical physics 9(11), 1276–1290 (2007).

[47] F. Tuinstra and J. L. Koenig, The Journal of Chemical Physics 53(3) (1970).

[48] M.S. Dresselhaus, G. Dresselhaus, R. Saito, and A. Jorio, Physics Reports 409(2), 47 – 99 (2005).

[49] R Saito, A Jorio, AG Souza Filho, G Dresselhaus, MS Dresselhaus, and MA Pimenta, Physical review letters 88(2), 027401 (2001).

[50] R Saito, A Grüneis, Ge G Samsonidze, VW Brar, G Dresselhaus, MS Dresselhaus, A Jorio, LG Cançado, C Fantini, MA Pimenta, et al., New Journal of Physics 5(1), 157 (2003).

[51] C Thomsen and S Reich, Physical Review Letters 85(24), 5214 (2000).

[52] J. Jiang, R. Saito, A. Grüneis, S. G. Chou, Ge. G. Samsonidze, A. Jorio, G. Dresselhaus, and M. S. Dresselhaus, Phys. Rev. B 71, 205420 (May 2005).

[53] J. Jiang, R. Saito, Ge. G. Samsonidze, S. G. Chou, A. Jorio, G. Dresselhaus, and M. S. Dresselhaus, Phys. Rev. B 72, 235408 (Dec 2005).

[54] J. Jiang, R. Saito, A. Grüneis, G. Dresselhaus, and M.S. Dresselhaus, Chemical Physics Letters 392(46), 383 – 389 (2004).

[55] G. G. Samsonidze. Photophysics of Carbon Nanotube. Ph. D. thesis, Massaschusetts Institute of Technology, Department of Physics, September 2007.

[56] L. G. Cançado, A. Jorio, and M. A Pimenta, Phys. Rev. B 76, 064304 (Aug 2007).